Milestone SP25CM3A

Saturated Zone Radionuclide Transport Model

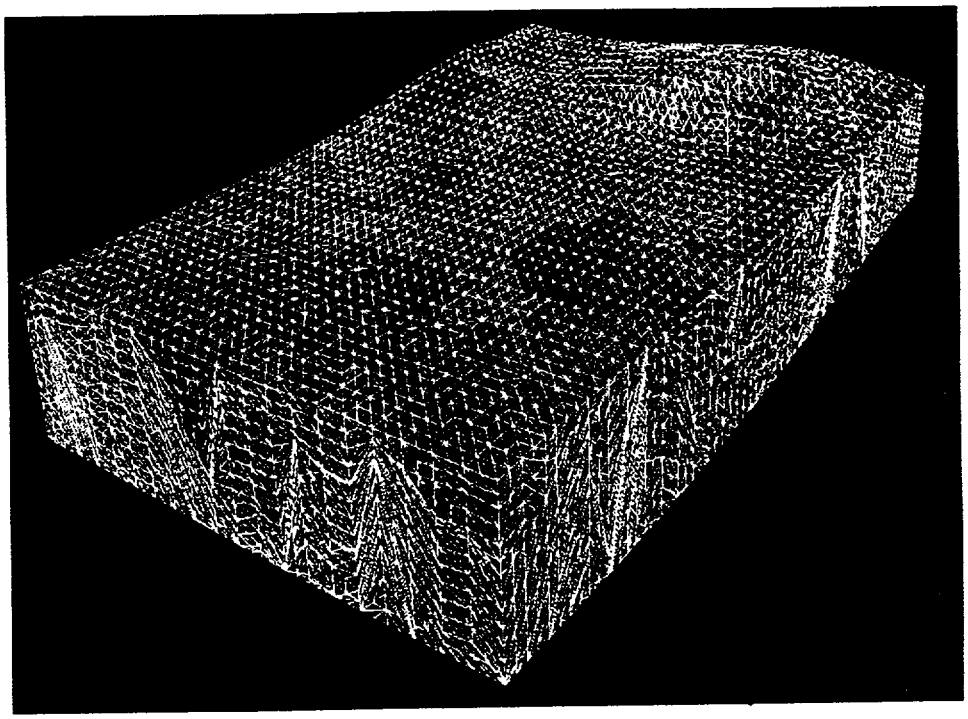

George A. Zyvoloski

Bruce A. Robinson

Kay H. Birdsell

Carl W. Gable

John Czarnecki

Kathy M. Bower

Claudia Faunt

September 29, 1997

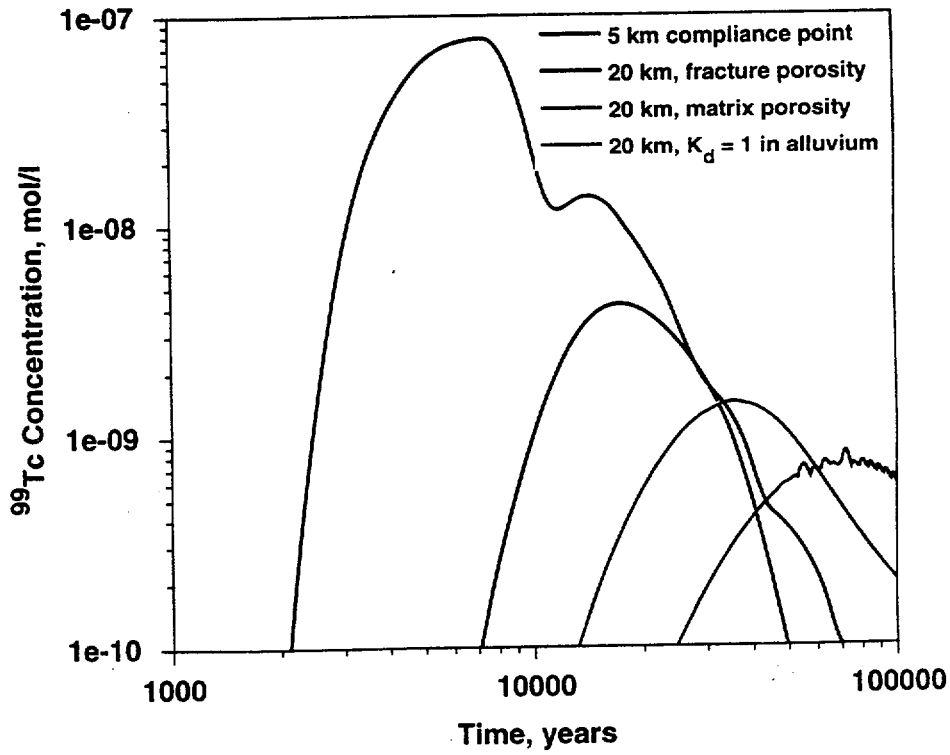

Los Alamos
NATIONAL LABORATORY

- Part 1

Acknowledgments

This work was supported by the Yucca Mountain Site Characterization Office as part of the Civilian Radioactive Waste Management Program. This project is managed by the U.S. Department of Energy, Yucca Mountain Site Characterization Project. The authors are grateful to a large number of people who contributed to this work. Harold Trease and Terry Cherry assisted in the preparation and testing of the numerical grids used in the model calculations. Bill Arnold provided the FEHM input files for the sub-site scale model developed at Sandia National Laboratories that was used in this report; Ines Triay consulted with us in the assignment of radionuclide sorption and diffusion coefficients; Hari Viswanathan assisted in the development of the transport module of FEHM and mapped the distribution of zeolites onto the sub-site scale model grid; June Fabryka-Martin provided valuable editorial comments on the Cl-36 modeling study; Claudia Faunt provided valuable assistance in characterization of the stratigraphic framework model and in providing figures depicting the model. Andy Wolfsberg performed a thorough review of the technical and editorial content of this report. Susan Klein, Roger Eckhardt, and Angela Sanchez-Pope provided considerable assistance in the editorial phase of the writing of this report, and helped compile the QA information. Finally, the authors are grateful to Lynn Trease for her assistance in preparing this document, and to the Los Alamos YMP Project office for their support during the course of this work.

QA Status of Software Used in This Report

The FEHM code is used to perform all flow and transport calculations in this report. The code is qualified in accordance with Los Alamos quality assurance requirements and is documented in (Zyvoloski et al., 1992, 1996a, 1996b). The petroleum industry standard software package STRATAMODEL is used in the building of the framework model. This is an off-the-shelf software package and an industry standard. It is non-Q with respect to YMP and Los Alamos

quality assurance requirements but follows well documented methods. The GEOMESH/X3D grid generation toolkit, (Gable et al., 1995, Trease et al., 1996) is non-Q with respect to YMP and Los Alamos quality assurance requirements. However, version control software tracking procedures identical to those used for the Q code FEHM are followed. GEOMESH/X3D utilizes well established procedures to insure robust mesh generation results and to insure traceability of changes to the software. A suite of test problems has been developed and all new releases are verified against the test suite.

Table of Contents

List of Figures

List of Tables

Chapter 1 - Executive Summary

An updated three-dimensional flow and transport model for the site-scale saturated zone (SZ) has been developed in a collaborative effort between the U.S. Geological Survey (USGS) and Los Alamos National Laboratory. The USGS is responsible for the flow model including the geological description, boundary conditions, and other compatibility conditions with the USGS regional-scale model. Los Alamos and USGS researchers have worked closely to insure that the finite-element grid accurately reflects the geological description and to obtain the initial steady-state flow solutions that are to become the basis for the parameter-estimation (PEST) runs. Los Alamos was responsible for grid generation and assisting the USGS in developing flow solutions. These flow simulations then become the basis for the radionuclide transport studies conducted at Los Alamos that are presented in this report. During this year's effort, several different framework models were constructed and many different grids were generated. The calibrated USGS/Los Alamos model is described in the USGS Milestone SP23NM3 (Czarnecki et al., 1997). Highlights from this year's effort on the saturated-zone flow and transport model are summarized in the following sections. The final section (Section 1.6) provides a road map between the requirements listed in the Criteria Statement for this milestone and the specific locations in the document where these requirements are met.

1.1 The FEHM Computer Code

To support the flow and transport modeling efforts for the saturated zone, several code enhancements to the computer code FEHM (Zyvoloski et al., 1996d) were made. First, an interface between FEHM and the commercial parameter-estimation software PEST (Watermark Computing, 1994) was developed. This feature allows the PEST software to be the driver for running multiple FEHM simulations in which parameter values are changed to fit the water-table elevation data. This method is far superior to manual fitting of data and is equivalent in functionality to the parameter-estimation codes being used for fitting other data sets in the Yucca

Mountain Site Characterization Project (YMP), such as MODFLOWP for the regional flow model and ITOUGH for the unsaturated zone. Other enhancements to the code include a reformulation of the saturated flow equations so that head is the primary variable rather than fluid pressure and minor changes to facilitate the accurate reporting of information on mass balance and fluid flow velocity. All of these changes aided in streamlining the execution of parameter sensitivity studies and examination of the results.

1.2 Summary of Site-Scale Flow Modeling Results

Although the details of the flow modeling effort are discussed in the USGS Milestone of Czarnecki et al. (1997), we summarize these results in the present study and elaborate on certain issues brought up in the Saturated Zone Expert Elicitation currently being conducted by the Yucca Mountain Site Characterization Project and in reviews of the Czarnecki milestone. A key concern addressed in the present study is the compatibility of the regional flow model of D'Agnese et al. (1997) and the site-scale flow model. Although, ideally, the output from the larger-scale regional model would be used as direct input to the site model, there are several factors that make such an interface impractical. First, the geologic model is defined in more detail at the site scale, so an exact piecing together of the models is impossible. Second, the regional model, focusing on larger-scale issues, does not have a detailed representation of geology near the site and does not attempt to include features such as the large hydraulic gradient in the calibration. Because of these differences, the models are compared with each other for consistency, rather than coupled more directly. In this chapter, we present results of a comparison of fluid flux exiting the south end of the site-scale model to the flux passing through the same region in the regional model. The calibrated site-scale model has a flux of 465 kg/s from the south face versus 323 kg/s over the same region for the regional model. This agreement is acceptable considering the compatibility issue raised above. Furthermore, the recharge and discharge flux values themselves, as input into the regional-scale model, have uncertainties that are larger than the computed difference of these two

models. Because the difference is within the range of uncertainty of the actual flux values, we consider the two models to be, for all intents and purposes, in agreement with one another.

Another flow issue addressed in the present study is the effect of temperature on the flow field and prediction of flux through the site-scale model. An analysis presented in this chapter shows that the model calibration is not significantly affected by the selection of 20°C for model calibration purposes. Computed heads differed by less than 1% between the system simulated assuming 40°C temperature and the system simulated assuming 20°C temperature. The difference in computed flux out of the south end of the model was somewhat larger but still well within the uncertainty range of the flux in the actual groundwater system. Therefore, we conclude that the calibrated model at 20°C is acceptable for the present study but recommend that, in future modeling, a more appropriate mean temperature be used to alleviate this concern.

Finally, in this chapter, we present a revised geologic description that will be used in future versions of the site-scale flow and transport model. The increased resolution of the model will allow for more accurate predictions of radionuclide migration from the footprint of the potential repository to the accessible environment. This geologic model, available in electronic form, will be used to construct a new numerical grid for flow and transport studies early in fiscal year 1998 (FY98).

1.3 Grid Generation and Grid Resolution Studies

Several three-dimensional grids were generated in support of the site-scale flow and transport modeling effort. Both structured and unstructured grids[1] were developed, tested, and used for sensitivity analyses and flow calibration studies. The hydrostratigraphy represented in the geologic model consists of multiple layers of contrasting fluid flow and transport properties. The grid-generation methods used in the present study allow the stratigraphy to be honored in numerical grids of different resolution so that comparison studies can be performed to test for grid quality and to determine the

1. Structured 3-D grids typically use hexahedra, lack adaptivity to complex geometries, but are easier to implement numerically than unstructured 3-D grids, which typically use tetrahedra.

resolution required for flow and transport simulations. All mesh generation and manipulation is done with the GEOMESH/X3D toolkit (Gable et al., 1995; Gable et al., 1996; Trease et al., 1996).

A series of six structured grids of increasing resolution were used to compare the flow through the model domain to assess the point at which increasing resolution no longer influences the results. This process identifies the resolution required for an accurate simulation of the flow field. A similar study for two unstructured grids demonstrated that the coarser grid used for calibrating the flow model was sufficiently resolved for accuracy. Finally, this chapter reports on the development of a technique for selectively refining the numerical grid for transport calculations. The method uses the solute transport pathway determined on a coarse grid to identify regions of the model where increased grid resolution is required. The mesh-generation software refines the grid in those areas. After two or more successive applications of this process, the grid is finely resolved along the pathways of solute plume movement, and numerical error associated with insufficient grid resolution is minimized. This technique is demonstrated in a simplified three-dimensional model, and the process is then described for the site-scale model grid. The main application of this technique will be for refining the revised site-scale model for transport calculations.

1.4 Saturated Zone Conceptual Model for Radionuclide Transport

The site-scale groundwater flow model provides the hydrologic framework for determining the direction and rate of movement of radionuclides reaching the saturated zone beneath Yucca Mountain. In addition to flow issues, the migration of radionuclides to the accessible environment depends on transport processes and parameters distinct from the flow model itself. This chapter develops a conceptual model for transport that includes advective transport of radionuclides, dispersion, diffusion of radionuclides from fractures into the rock matrix, and sorption. Within the fractured tuffs, the migration of radionuclides is expected to be primarily through regions with higher bulk fracture permeability. Flow within individual joints probably occurs through channels,

rather than as sheet flow through parallel-plate fractures. At more distant downstream locations, the migration is likely to be through alluvium, and a model for flow and transport through a porous continuum, rather than fractured rock, is likely to apply.

For transport in porous, fractured tuff, radionuclides can escape the fractures by diffusion into the rock matrix. Such diffusion is a significant retardation mechanism that is likely to provide a benefit to performance. There have been several theoretical, laboratory, and field studies pointing to the validity of matrix-diffusion models. Of greatest relevance are the interwell tracer experiments at the C-Wells (Reimus and Turin, 1997) and the recently reported Nevada Test Site experiment of Waddell (1997). Both of these experiments used tracers with different diffusion coefficients to investigate whether differences in breakthrough curves could be detected in accordance with matrix-diffusion model predictions. The results of both tests point to the validity of the matrix-diffusion model for transport through fractured tuffs.

The degree of matrix diffusion detected in field tracer tests is small, due to the short time scales in forced-gradient transport tests, compared to transport in groundwater under natural conditions. A theory is developed to estimate the impact of matrix diffusion on radionuclide migration in the saturated zone away from Yucca Mountain. We show that transport can be approximated using an effective transport porosity that, in general, falls between the fracture porosity and the porosity of the surrounding rock matrix. The key factors controlling this effective porosity are the groundwater flow velocity, travel distance, matrix diffusion coefficient, and mean spacing between flowing fractures. For transport in the saturated zone, effective porosities are apt to be much larger than the fracture porosity, approaching the matrix porosity under some circumstances. This effect leads to radionuclide travel times on the order of thousands of years compared to times on the order of one year if radionuclides are confined to the fractures. The matrix diffusion model is shown to be consistent with ^{14}C ages measured for saturated-zone fluids, although the data do not rule out some differences in concentration between fracture and matrix fluids. A possible exception to the result of travel times in the thousands of years is colloid-

facilitated transport of plutonium. This possibility is addressed with a mathematical model developed in this chapter that includes sorption to mobile colloids.

Dispersion is caused by heterogeneities at all scales from the pore scale to the scale of the thickness of individual strata and the length of structural features such as faults. The resulting spreading of radionuclides is important to performance and must be captured in transport models. Only the largest heterogeneities are represented explicitly in the site-scale model; all dispersion caused by smaller-scale features must be represented through the use of a dispersion model. Numerous groundwater transport studies have been conducted at a variety of scales, and the results are compiled using the dispersivity as the correlating parameter. It is well-known that dispersivity increases with the scale, or distance, of transport of a solute. The only site-specific data come from the C-Wells reactive tracer experiment of Reimus and Turin (1997) and accompanying tracer tests carried out by the USGS at the C-Wells. These experiments yielded estimated dispersivity values that fall in the range of uncertainty of correlations to data collected and compiled at many sites. This result provides credibility that the dispersivity values used in the field simulations are appropriate.

1.5 Transport Results

Several models and numerical techniques are used to obtain results for radionuclide transport in the saturated zone. First, a technique based on numerical convolution is developed to link the unsaturated-zone breakthrough curves at the water table to the saturated-zone transport system. In this method, the inputs are the mass flux of radionuclide reaching the water table versus time, along with a generic breakthrough curve in the saturated zone computed as the response at a downstream location to a constant injection of radionuclide at the footprint of the proposed repository. The numerical implementation of the method was verified by performing a full calculation using the actual time-varying input from an unsaturated-zone calculation as input to the saturated-zone model. The method allows a variety of input flux curves to be computed quickly

without recomputing the saturated-zone calculation each time. Assumptions inherent to the convolution technique include steady-state flow and linear transport processes.

Before proceeding to more complex site-specific models, we present a simplified three-dimensional flow and transport model to examine the importance of several transport parameters that are difficult to investigate fully with the current site-scale models. Dispersivity is established as one of the key uncertain parameters that influence the concentration (and hence dose) at accessible-environment compliance points. The transverse dispersivity is actually a more sensitive parameter for dilution because it governs the degree of lateral spreading of the plume. Matrix diffusion, established as a valid process in field test of Reimus and Turin (1997), affects the breakthrough times at a downstream location but, to a first approximation, does not influence the peak concentration. Another important factor regarding matrix diffusion is that it allows radionuclides to contact minerals in the rock matrix that potentially sorb radionuclides. Even small amounts of sorption have a large effect on breakthrough times and peak concentrations. Finally, this simplified model was used to illustrate that the saturated-zone transport system has the ability to dilute spikes of high concentration and short duration that come from bypassing of the unsaturated zone through fractures. Thus, the saturated zone provides an important component in a "defense-in-depth" strategy in which uncertainties leading to poor performance in one part of the repository system are mitigated by the performance of another radionuclide transport barrier.

To simulate radionuclide transport from the footprint of the repository to a 5-km compliance point, we used a sub-site scale model developed at Sandia National Laboratories (Ho et al., 1996). This model was chosen as an appropriate substitute to performing these calculations using the site-scale model because of the more accurate representation of the geology near Yucca Mountain. When the site-scale model is revised to use the new hydrostratigraphic data based on a 250 x 250-m geologic grid, all calculations will be performed with the site-scale model itself. The sub-site scale-model flow results capture the large hydraulic gradient and flow through the geologic strata of relevance downstream of the repository footprint, including the Prow Pass, Bullfrog, and Tram Tuffs units. Radionuclides travel to the east and south from the footprint to a

5-km compliance point. Releases into the Prow Pass unit travel in a more easterly direction than releases in the other units; releases into the Tram unit at the south end of the footprint travel almost due south. All releases follow the dipping stratigraphy, indicating downward movement of radionuclides. This effect may be important if upcoming field studies reveal more reducing conditions with depth, because sorption coefficients of ^{99}Tc and ^{237}Np are likely to be much higher and solubilities much lower under reducing conditions.

Transport times to a hypothetical 5-km compliance point under conditions in which the effective porosity is the matrix porosity are on the order of a few thousand years; much shorter transport times result from an assumption of less matrix diffusion. However, the extent of matrix diffusion itself only influences the arrival time rather than the concentration at the downstream location. This effect is in contrast to differences in fluid flux that may occur due to future wetter climates, which result in earlier travel times but also lower concentrations (greater dilution). Sorption of radionuclides such as ^{237}Np onto zeolitic tuffs in the saturated zone also leads to significant retardation and longer travel times to the 5-km compliance point.

The results of the sub-site scale model are then used as input to transport calculations to a hypothetical 20-km compliance point in the site-scale model. Simulations assuming both fracture-like and matrix-like effective porosities in the fractured tuff were performed to investigate the importance of this parameter. In both simulations, the alluvium present along the transport pathways were assigned high porosity. In this set of calculations, the nature of transport in the fractured tuffs is less important as the system becomes increasingly dominated by long predicted travel times in the alluvium. Thus, even if the tuffs are presumed to have a low effective porosity, travel times of 10 ky or more are predicted in the alluvium alone. Furthermore, we show that even small amounts of sorption in the alluvium shift travel times to values on the order of 50 ky, and predicted concentrations at the compliance point are lower than in the absence of sorption. Clearly, for more distant compliance points, the flow and transport behavior of the alluvium becomes increasingly the controlling factor in saturated-zone performance.

The influence of repository heat on saturated-zone flow and transport of radionuclides is also studied using the sub-site scale model. Repository waste heat creates a zone of higher-than-ambient temperature that extends vertically into the saturated zone and along the prevailing flow pathway from the repository. However, the predicted impact on transport of ^{99}Tc to the 5-km compliance point is very small. One outstanding issue related to repository heat is the possibility of temporary or durable changes to the permeability and porosity due to temperature-dependent rock-water interactions. If these effects turn out to be minor, then we can conclude that repository waste heat has minimal influence on the migration of radionuclides through the saturated zone.

Integrated transport predictions are presented in which we link the unsaturated-zone transport model of Robinson et al. (1997) with the sub-site scale model developed in the present study to predict the transport of the key radionuclides ^{99}Tc, ^{237}Np, and the isotopes of plutonium. In Robinson et al. (1997), we investigated the performance of the unsaturated-zone system for different infiltration rates that could result from changes to the present-day climate. These predictions of radionuclide mass flux at the water table are input to convolution calculations to predict the combined unsaturated/saturated-zone performance at 5 km. For the unsaturated-zone performance predicted in Robinson et al. (1997), the integrated response in the saturated zone for ^{237}Np and ^{99}Tc are a direct consequence of dilution of percolating unsaturated-zone fluid with flowing saturated-zone groundwater. Therefore, poorer performance predicted for the unsaturated zone under wetter future-climate scenarios translates directly to higher predicted concentrations in the saturated zone. Sorption onto zeolites in the saturated zone should provide a considerable delay in arrival times for ^{237}Np. For plutonium, rather than climate change or sorption to the host rock, the key factor influencing concentrations is the propensity of plutonium to sorb to mobile colloids.

Regarding the nature of flow and transport in the fractured tuffs, we experimented with different flow and transport models to investigate different methods of simulating this dual-porosity system. A dual-porosity particle-tracking model for transport was invoked, and the influence of matrix diffusion properties was examined. The results follow those of the matrix-

diffusion conceptual model, but several factors argue against its use in large-scale transport model predictions. First, the particle-tracking module does not, at present, handle the dispersion-coefficient tensor formulated as longitudinal and transverse components. Furthermore, although the diffusion model accurately simulates the case of diffusion into an infinite matrix continuum, finite fracture spacings are not part of the model as currently constituted. Therefore, particle tracking cannot be used in site-scale models. A finite-element dual-porosity solution was also investigated. As expected, the dual-porosity flow simulation yielded virtually identical steady-state results to the single-continuum model. Transport results captured the two extremes (fracture-dominated and pervasive matrix diffusion) well but failed to produce accurate results for small but non-negligible diffusion into the rock matrix. We therefore recommend that an appropriate abstracted transport model employ the effective porosity concept, with theoretical relationships involving matrix diffusion and fracture spacing parameters used to set the transport porosity throughout the model domain.

1.6 Traceability to Criteria for Milestone SP25CM3A

The table below provides a road map between the requirements listed in the Criteria Statement for this milestone and the specific locations in the document where these requirements are met.

Table 1-1. Criteria Statement Requirements and Location in the Milestone SP25CM3A

Criterion	Location in Milestone
This report will include a conceptual model of the transport of radionuclides in the saturated zone down gradient from Yucca Mountain to the accessible environment...	Conceptual model for radionuclide transport in the saturated zone: Chapter 5.

Table 1-1. Criteria Statement Requirements and Location in the Milestone SP25CM3A

Criterion	Location in Milestone
including 2- and 3-D integrated transport calculations and sensitivity analyses.	3-D integrated transport calculations: all simulations performed in three dimensions because 2-D calculations are insufficient to capture the relevant processes. Integrated transport calculations: Sections 6.13 and 6.14. Sensitivity analyses: Sections 6.4, 6.7, 6.11, 6.12, 6.13, 6.14, and 6.15.
Both equivalent-continuum and dual-permeability calculations will be made...	Dual permeability: Section 6.15. Equivalent continuum: the rest of Chapter 6.
incorporating discrete structural features as available and appropriate.	Site-scale model: 6.10. Sub-site scale model: 6.6 (low-permeability faults).
The model will do the following:	
Incorporate and consider isotopic data that are indicative of processes and rates of fluid flow or residence times in the saturated zone.	Section 5.5.
Draw upon the Report on Summary of Geochemistry/Transport Laboratory Tests to provide defensible values for important transport processes and parameters including:	
sorption...	Sections 6.4, 6.7, 6.13.2, and 6.14.
and diffusion coefficient;	Sections 5.6 and 6.15.1.
radionuclide solubility and speciation;	Section 6.13.
and colloids as controlled by relevant thermal effects and water chemistry.	Sections 5.5.4 and 6.13.3.
Particular attention will be paid to the potential for dilution in the saturated zone.	Sections 5.5.3, 6.4, 6.11.1, and 6.13.
Results from C-wells reactive and conservative tracer tests will be used for confidence building in transport calculations.	Sections 5.5.2, 5.5.3, and 5.5.4.
Rely heavily on input from the 3-D mineralogical model of Yucca Mountain.	Section 6.7.
Update 3-D transport simulations for radionuclides including, but not limited to:	

Table 1-1. Criteria Statement Requirements and Location in the Milestone SP25CM3A

Criterion	Location in Milestone
Np;	Sections 6.13.2 and 6.14.
Pu;	Section 6.13.3.
Tc;	Sections 6.12, 6.13.1, and 6.14.
under ambient...	Sections 6.11, 6.13, and 6.14
and thermally perturbed scenarios;	Section 6.12
for two future climates and accompanying infiltration fluxes and effects on recharge.	Sections 6.11.1, 6.13, and 6.14.
The report will be coupled to output from the Unsaturated Zone Site Transport Model, which will provide fluxes of water and radionuclides to the saturated zone.	Sections 6.3, 6.9, 6.12, and 6.13.
The deliverable will be prepared in accordance with OCRWM-approved quality assurance procedures implementing requirements of the Quality Assurance Requirements Description.	Done.
The product shall be developed on the basis of the best technical data, including both Q and non-Q data. The Q status of data used and cited in the report shall be appropriately noted.	See QA tables in document.
Stratigraphic nomenclature used shall be consistent with the Reference Information Base section 1.12(a): Stratigraphy-Geologic Lithologic Stratigraphy.	Section 3.6, Table 3-2.
References to data used in the report shall include record Accession Numbers or Data Tracking Numbers when available.	See QA tables in document.
Technical data contained within the deliverable and not already incorporated in the Geographic Nodal Information Study and Evaluation System (GENISES) shall be submitted for incorporation into the GENISES in accordance with YQP-SIII.3Q.	N/A.

Table 1-1. Criteria Statement Requirements and Location in the Milestone SP25CM3A

Criterion	Location in Milestone
Verification of technical data submittal compliance shall be demonstrated by including as part of the deliverable:	
a) A copy of the Technical Data Information Form generated identifying the data in the Automated Technical Data Tracking system, and...	N/A.
b) a copy of the transmittal letter attached to the technical data transmittal to the GENISES Administrator.	Done.

Chapter 2 - General Description of the FEHM Computer Code

2.1 Summary

To support the flow and transport modeling efforts for the saturated zone, several code enhancements to the computer code FEHM (Zyvoloski et al., 1996d) were made. First, an interface between FEHM and the commercial parameter-estimation software PEST (Watermark Computing, 1994) was developed. This feature allows the PEST software to be the driver for running multiple FEHM simulations in which parameter values are changed to fit the water-table elevation data. This method is far superior to manual fitting of data and is equivalent in functionality to the parameter-estimation codes being used for fitting other data sets in the YMP, such as MODFLOWP for the regional flow model and ITOUGH for the unsaturated zone. Other enhancements to the code include a reformulation of the saturated flow equations so that head is the primary variable rather than fluid pressure as well as minor changes to facilitate the accurate reporting of information on mass balance and fluid flow velocity. All of these changes aided in streamlining the execution of parameter sensitivity studies and examination of the results.

2.2 Software and Data QA Status

The FEHM code is used to perform all flow and transport calculations in this report. The code is qualified in accordance with Los Alamos quality-assurance requirements and is documented in Zyvoloski et al. (1992, 1996b, 1996c).

2.3 Introduction

The FEHM (Finite Element Heat and Mass) (Zyvoloski et al., 1996c) computer code is used to simulate flow and transport through both the unsaturated and saturated zones. FEHM is a nonisothermal, multiphase flow and transport code. It simulates the flow of water and air and the

transport of heat and solutes in two- and three-dimensional saturated or partially saturated, heterogeneous porous media. The code includes comprehensive reactive geochemistry and transport modules and a particle-tracking capability. Fractured media can be simulated using an equivalent-continuum, discrete-fracture, dual-porosity, or dual-permeability approach.

FEHM was developed at Los Alamos National Laboratory with the support of a variety of sponsors, including the Yucca Mountain Site Characterization Project (YMP). FEHM has undergone extensive validation and verification as part of the YMP (Dash et al., 1996b). The computer code has been certified in accordance with the LANL YMP Software QA program. FEHM is coupled to a sophisticated grid-generation package that generates accurate and realistic meshes from hydrostratigraphic databases.

The basic conservation equations, constitutive relationships, and numerical methods in FEHM are described here. Additional information is given in Reeves (1994), Zyvoloski et al. (1996a–d), and Dash et al. (1996a–c).

2.4 Conservation Equations

FEHM solves three mass conservation equations: conservation of total fluid mass (air and water), conservation of air, and conservation of solute (contaminant). The mass of the solute is assumed to be small enough not to affect the total fluid mass balance or fluid properties. When evaporative or thermal processes are being simulated, a fourth conservation equation is necessary: conservation of energy. In this report, the full set of equations is not being used. The following summarizes the limited flow physics used for the saturated zone. In most of the simulations in the present study, isothermal calculations were carried out. This is appropriate for the calibration work of the USGS and the transport simulations reported here. Next year, temperatures will likely be used to refine the calibration effort. Thus, we include the thermal equations in this summary.

Conservation of total fluid mass is expressed by the equation:

$$\frac{\partial A_m}{\partial t} + \nabla \bullet f_m + q_m = 0 \quad , \qquad \text{(Eq. 2-1)}$$

where the subscript m refers to the mass and where the mass per unit volume, A_m, is given by

$$A_m = \phi(\rho_l) \quad , \qquad \text{(Eq. 2-2)}$$

and the mass flux, f_m, is given by

$$f_m = \rho_l v_l \quad , \qquad \text{(Eq. 2-3)}$$

where:

ϕ = porosity of the matrix,

ρ_l = density for the liquid phase,

v_l = velocity for the liquid phase, and

q_m = source and sink term (such as wellbores).

Conservation of energy is expressed by the equation:

$$\frac{\partial A_e}{\partial t} + \nabla \bullet f_e + q_e = 0 \quad , \qquad \text{(Eq. 2-4)}$$

where the subscript e refers to the energy and where the energy per unit volume, A_e, is given by

$$A_e = (1-\phi)\rho_r u_r + \phi(\rho_l u_l) \quad , \qquad \text{(Eq. 2-5)}$$

where $u_r = c_p T$ and the energy flux, f_e, is given by

$$f_e = \rho_l h_l v_l - K\nabla T \quad , \qquad \text{(Eq. 2-6)}$$

where:

u_r, u_l = internal energy of the rock matrix and the liquid phase, respectively,

ρ_r, ρ_l = density for the rock matrix and the liquid phase, respectively,

c_p = specific heat (subscript p refers to constant pressure),

h_l = specific enthalpy for the liquid phase,

K = effective thermal conductivity of the saturated rock matrix,

T = temperature, and

q_e = energy contributed from sources and sinks.

It is assumed that Darcy's Law applies to the movement of fluid:

$$v_l = -\frac{k_s}{\mu_l}(\nabla P_l - \rho_l g) \quad , \qquad \text{(Eq. 2-7)}$$

where:

k_s = saturated permeability,

μ_l = viscosity for the liquid phase,

P_l = phase pressure for the liquid phase, and

g = acceleration due to gravity.

For simplicity, the equations are shown for an isotropic medium, though this restriction does not exist in the FEHM computer code.

Using Darcy's Law, the basic conservation of mass and energy equations can be rewritten as:

$$-\nabla\bullet(D_{ml}\nabla P_l) + q_m + \frac{\partial}{\partial z}g(D_{ml}\rho_l) + \frac{\partial A_m}{\partial t} = 0 \qquad \text{(Eq. 2-8)}$$

and

$$-\nabla\bullet(D_{el}\nabla P_l)-\nabla\bullet(K\nabla T)+q_e+\frac{\partial}{\partial z}g(D_{el}\rho_l)+\frac{\partial A_e}{\partial t}=0\quad , \qquad \text{(Eq. 2-9)}$$

where z is oriented in the direction of gravity. Here the transmissibilities are given by

$$D_{ml}=\frac{k_s\rho_l}{\mu_l} \qquad \text{(Eq. 2-10)}$$

and

$$D_{el}=h_l D_{ml}\quad . \qquad \text{(Eq. 2-11)}$$

The conservation of solute equation is not directly coupled to the flow (pressure) field. The source or sink strength, q_c, and accumulation term, A_c, are defined as follows for the solute conservation equation:

$$\begin{aligned} q_c &= C_l q_m \\ A_c &= \phi(C_l\rho_l) \end{aligned} \quad , \qquad \text{(Eq. 2-12)}$$

where C_l is the concentration of the solute (contaminant) in the liquid phase.

The conservation equation for a given solute is given by

$$-\nabla\bullet(C_l D_{ml}\nabla P_l)-\nabla\bullet(D_{cl}\nabla C_l)+ \qquad \text{(Eq. 2-13)}$$
$$q_c+\frac{\partial}{\partial z}g(C_l D_{ml}\rho_l)+\rho_r\frac{\partial C_r}{\partial t}+\frac{\partial A_c}{\partial t}=0\quad .$$

Here $\nabla\bullet(D_{cl}\nabla C_l)$ is the solute dispersion term, $\rho_r\partial C_r/\partial t$ is the adsorption term, and C_r is a concentration representing the adsorption of a solute onto the porous media. FEHM supports several adsorption models. For the simulations discussed in this report, a simple linear model is used: $C_r = K_D C_l$, where K_D is the distribution coefficient. In addition, the reactive transport module contains rock/solute interactions and aqueous speciation reactions. These features are not used in the present study. For a complete description, see Robinson et al. (1997) and Viswanathan et al. (1997).

2.5 Constitutive Relationships

FEHM requires information about water properties (and their derivatives) as functions of temperature (T) and pressure (P). Rational-function approximations are used to estimate these properties in FEHM, where the rational functions are a ratio of polynomials. For water, polynomial coefficients were obtained by fitting data from the database used for the NBS/NRC Steam Tables (Harr et al., 1984).

2.6 FEHM Code Changes in Support of the Saturated Zone Flow Model

Several code changes were made to FEHM this year in support of the SZ modeling effort. These include a formulation based on hydraulic head rather than absolute pressure, an interface to the parameter-estimation program PEST (Watermark Computing, 1994), calculation of internode velocities, revised mass-balance calculations for Dirichlet (fixed head) boundary conditions, and a Boussinesq approximation. The hydraulic head option has been used successfully in the PEST calibration runs and has been a useful tool for comparing with field measurements. The PEST interface has helped in the USGS calibration effort by providing a straightforward and error-free communication with the PEST code. The internode velocity output, which previously used interpolated FEHM data to derive a finite-element-based velocity, now uses a method that outputs FEHM information directly. With this change, the graphical results near boundaries and permeability contrasts are now much more realistic. The improved mass-balance calculation for fixed boundary conditions improved the calculations of flux from boundaries. The Boussinesq formulation that was added to FEHM approximates the density in the flow terms as a constant while retaining the pressure dependence in the accumulation term. This change allows for hydraulic head calculations and leads to little error in the results.

2.7 Numerical Methods

FEHM uses a finite-element/ finite-volume method to discretize the conservation equations. This method allows for the numerical efficiency of finite-difference methods while retaining the geometric modeling capabilities of finite-element methods (see Zyvoloski (1983) and Fung et al. (1992) for details). Newton-Raphson iteration is applied to the fully coupled system of equations. This system of equations is solved with multi-degree of freedom, preconditioned, conjugate gradient methods, using the GMRES technique or the biconjugate gradient squared acceleration technique.

2.8 Solution Procedure for Steady-State Flow Problems

The calibration of the flow solution reported in Czarnecki et al. (1997) was obtained by using the FEHM code with the PEST parameter-estimation software. Likewise, the assembling of all relevant data and grid generation are also described in that report. Because of the incorporation of the potentiometric surface into the grid, the problem is fully saturated and modeled as though the saturated zone is a confined aquifer. This condition means that the equations are linear while retaining the large contrasts in permeability. The FEHM code was run in reduced degree-of-freedom mode, which means that the full two-phase solution was simplified to a one-phase (saturated) solution where applicable but still allowed for two-phase behavior should that become necessary. The steady-state solution for heads was accomplished by running the FEHM code in transient mode and stopping the calculation when the time-step was large and the inflow equaled the outflow. This condition occurred in as few as one time-step. Multiple time-steps were sometimes necessary for permeability fields with large variability. CPU times, including I/O, were usually less than one minute.

2.9 Conclusions

The FEHM code proved to be an efficient and flexible tool for obtaining flow and transport solutions for the YMP site-scale saturated-zone modeling effort. Modifications made to FEHM provided a seamless link to the parameter-estimation code PEST for performing parameter-estimation calculations.

Chapter 3 - Summary of Site-Scale Flow Modeling Results

3.1 Summary

Although the details of the flow modeling effort are discussed in the USGS milestone of Czarnecki et al. (1997), we summarize these results in the present study and elaborate on certain issues brought up in the Saturated Zone Expert Elicitation and reviews of the Czarnecki milestone. A key concern addressed in the present study is the compatibility of the regional flow model of D'Agnese et al. (1997) and the site-scale flow model. Although, ideally, the output from the larger-scale regional model would be used as direct input to the site model, there are several factors that make such an interface impractical. First, the geologic model is defined in more detail at the site scale, so an exact piecing together of the models is impossible. Second, the regional model, focusing on larger-scale issues, does not have a detailed representation of geology near the site and does not attempt to include features such as the large hydraulic gradient in the calibration. Because of these differences, the models are compared with each other for consistency, rather than coupled more directly. In this chapter, we present results of a comparison of fluid flux exiting the south end of the site-scale model to the flux passing through the same region in the regional model. The calibrated site-scale model has a flux of 465 kg/s from the south face versus 323 kg/s over the same region for the regional model. This agreement is acceptable considering the compatibility issue raised above. Furthermore, the recharge and discharge flux values themselves, as input into the regional-scale model, have uncertainties that are larger than the computed difference of these two models. Because the difference is within the range of uncertainty of the actual flux values, we consider the two models to be, for all intents and purposes, in agreement with one another.

Another flow issue addressed in the present study is the effect of temperature on the flow field and on the prediction of flux through the site-scale model. An analysis presented in this chapter shows that the model calibration is not significantly affected by the selection of 20°C for

model calibration purposes. Computed heads differed by less than 1% between the system simulated assuming 40°C temperature and the system simulated assuming 20°C. The difference in computed flux out of the south end of the model was somewhat larger but still well within the range of uncertainty of the flux in the actual groundwater system. Therefore, we conclude that the calibrated model at 20°C is acceptable for the present study but recommend that, in future modeling, a more appropriate mean temperature be used to alleviate this concern.

Finally, in this chapter, we present a revised geologic description that will be used in future versions of the site-scale flow and transport model. The increased resolution of the model will allow for more accurate predictions of radionuclide migration from the footprint of the potential repository to the accessible environment. This geologic model, available in electronic form, will be used to construct a new numerical grid for flow and transport studies early in FY98.

3.2 Software and Data QA Status

The FEHM code is used to perform all flow and transport calculations in this report. The code is qualified in accordance with Los Alamos quality-assurance (QA) requirements and is documented in several reports by Zyvoloski et al. (1992, 1996b–d). The QA status of the data used in this report is shown in Table 3-1.

Table 3-1. QA Status of Data used in this Chapter

REFERENCE	QA Status	DTN/ Assession Number	COMMENT
Ciesnik, M. S. 1995. Groundwater altitudes and well data, Nye County, Nevada, and Inyo County, California. USGS open file report 93-89.	non-Q	MOL.19940908.0070	
Czarnecki, J. B., et al. 1997. Preliminary three-dimensional finite-element groundwater flow model of the saturated zone, Yucca Mountain, Nevada. USGS YMP milestone number SP23NM3.	non-Q		
Clayton, R. W., et. al. 1997. ISM2.0: A 3-D geological framework and integrated site model of Yucca Mountain: Version ISM1.0, Doc ID B00000000-01717-5700-00004, Rev. 0, MOL. 19970122.0053. CRWMS M&O.	Q		By agreement with DOE and NRC, accepted as Q even though it uses some non-Q data
Zelinski, W. P., and R. W. Clayton. 1996. A 3-D geological framework and integrated site model of Yucca Mountain: Version ISM1.0, Doc ID B00000000-01717-5700-00002, Rev. 1. CRWMS M&O,	non-Q		
D'Agnese, F.A., et al. 1997. Hydrogeologic evaluation and numerical simulation of the Death Valley regional groundwater flow system, Nevada and California, using geoscientific information systems. U.S. Geological Survey Water Resources investigations report 96-4300 (in press).	non-Q		

3.3 Introduction

In this chapter, we review the ongoing development of the site-scale flow model on which subsequent transport simulations will be performed. The development of the stratigraphy and

steady-state, calibrated flow solution is a collaborative effort involving the USGS and Los Alamos. Details of the hydrostratigraphic delineation and calibrated flow solutions is the subject of USGS milestone SP23NM3 (Czarnecki et al., 1997). The purpose of this chapter is to provide a brief update on outstanding issues that are being resolved as of the writing of this milestone. These include comparisons of the site-scale and regional-scale model, the influence of temperature on the calibrated flow results, and a brief discussion of the new hydrostratigraphic model on which an updated version of the site-scale model will be constructed early in FY98.

3.4 Regional-Scale/Site-Scale Model Interface

The form of the flow boundary conditions employed in obtaining a calibrated model plays a large role in the model results, especially with respect to subsequent transport predictions. A model calibrated to measured head values is a nonunique solution that must be constrained with measured or estimated flux values at boundaries. Simply put, if only head boundary conditions are used, the total flux is directly proportional to the values of permeability in the model; increasing or decreasing each permeability value by a fixed ratio changes the total flux by that same fraction. At the site scale, the flux values into and out of the flow domain cannot be directly tied to major recharge and discharge values because these occur outside the model domain. Because this is the case, there is a need to tie the flux values into and out of model faces to a larger-scale model. In this year's effort, there is a strong interplay between the calibrated regional model of D'Agnese et al. (1997) and the site-scale model of Czarnecki et al. (1997). In this section, we present results of a comparison of flux values predicted by the two models.

The original plan for the site-scale model was to use fluxes or head data from the regional model as boundary conditions for the site-scale model. However, there are several problems in applying fluxes directly. The first is that the site model has sixteen units represented within its boundaries, whereas the regional-scale model represents only three units in this region. This difference presents problems in assigning fluxes to nodes with widely varying permeabilities. The

second problem is that the calibrated heads for the regional model deviated the most from well data near the northern boundary of the site-scale model. Thus, fluxes were apt to be most inaccurate in that region. Because of these problems, the fixed head boundary conditions were derived from measured head data. Because of the fixed head conditions, solutions are valid for permeability ratios only. Fluxes must therefore be compared to those predicted by the regional-scale model to insure consistency.

Because of the need for finer resolution (primarily in the z direction), the site-scale model was developed with a smaller horizontal extent than previous site-scale models. The model dimensions are approximately 30 km by 45 km. The model boundary and hydrogeologic setting are shown in Figure 3-1. The compilation of all relevant data was done by the USGS, and these data were then organized into a Stratigraphic Framework Model (SFM). The SFM provided the basis for all grid generation. The grid building effort produced 15 grids this year for testing. The grid used in the calibration was on a 1500 x 1500 m areal spacing that consisted of 5485 nodes, 29,760 elements, and 40,548 internode connections. The calibration of this model is described in Czarnecki et al. (1997). A good calibration on an initial modeling exercise was obtained, but large flux values pointed to a systematic error in the geometric part of the flow terms. This problem was subsequently corrected, and the flow results revealed more realistic fluxes. The corrected model results were performed on a grid containing 9279 nodes, 52,461 elements, and 67,324 internode connections. The increase in the number of nodes was due to the inclusion of model "buffer zones" that play no part in the solution but improve the definition of the potentiometric surface (Figure 3-2). These zones are assigned values of zero for both porosity and permeability and, therefore, do not enter into the fluid flow calculation. Only the layers sandwiched between the upper and lower buffer zones are part of the flow model itself. The calibrated model produced with the mesh shown on Figure 3-2 was very good with the largest residuals being for the observation wells in the Forty Mile Wash. A discussion is given by Czarnecki et al. (1997). The majority of residuals were less than 5 m, though some of the Forty Mile Wash residuals were in the 30 m range. One observation well in the Forty Mile Wash area and in the Large Hydraulic Gradient region had an

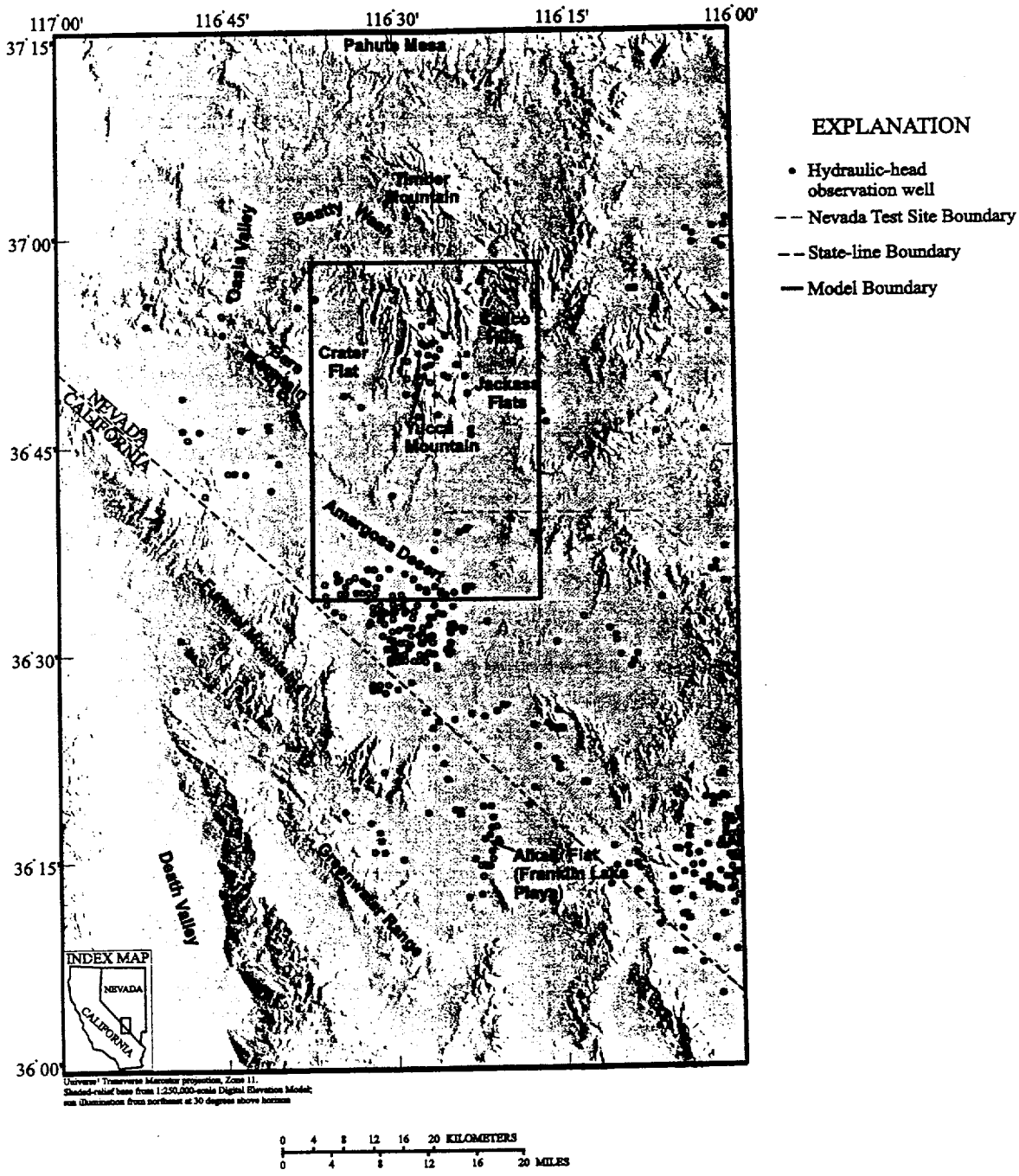

Figure 3-1. Geographic setting, model domain, and location of observation wells.

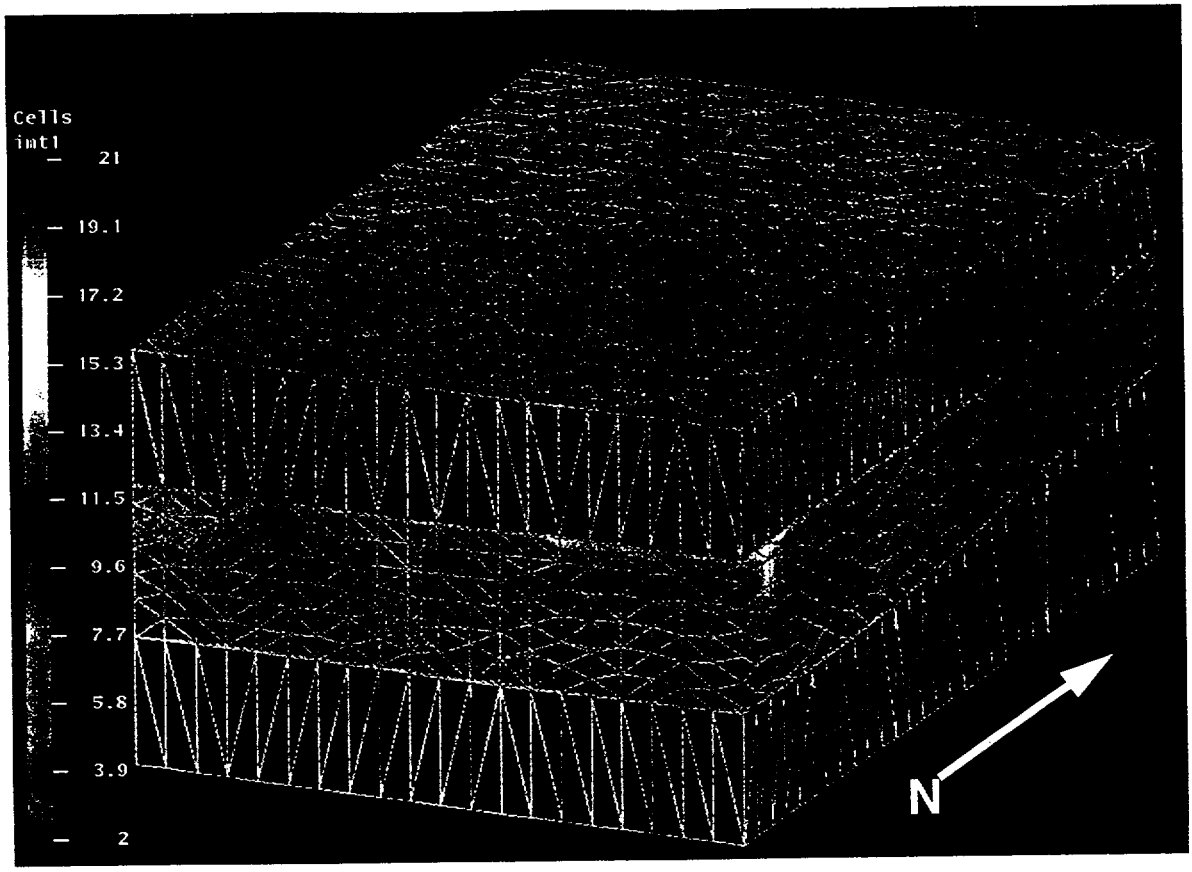

Figure 3-2. Saturated-zone computational model with buffer zones added above the potentiometric surface and below the bottom surface for the calculations.

observed head of 1187 m, whereas the simulation produced a head of 1057 m. This was (by far) the worst match and, not unexpectedly, in the area of most uncertainty. This model could be further improved by adjusting fluxes in the Forty Mile Wash region, but such an effort may not be warranted as the computation in FY98 will be with the higher resolved 250-m framework model described in Section 3.5.

There are difficulties in directly comparing the flux values in the site-scale and regional models. First, they are based on different hydrogeologic descriptions and unit delineations. By necessity, the regional model has a more averaged unit delineation than does the site-scale model. Furthermore, it is difficult to compare the fluxes from several faces of the model because the large hydraulic gradient is not represented in the regional-scale model, whereas the north and east sides

of the site-scale model were strongly influenced by inclusion of the large hydraulic gradient. Nevertheless, flow out of the south face of the site-scale model has a value of 465 kg/s compared to flow out of the same face in the regional model of 323 kg/s. This comparison illustrates that there is a reasonable correspondence between the models.

It is important to understand the effect of temperature on the flow and transport in the saturated zone where the density and viscosity depend on temperature. Over the range from 20 to 40°C, minimum and maximum temperatures in the saturated zone near Yucca Mountain, the density decreases about one percent whereas the viscosity decreases about fifty percent. To test the impact of temperature, two runs were made: one using an average saturated-zone water temperature of 20°C and another using an average saturated-zone water temperature of 40°C. The comparison of measured and computed heads were compiled by choosing a node within each of the sixteen units. The average head changes were computed with these nodes by using the absolute value of the difference between the solutions. A value of 4.83 m was obtained, less than a percent change in the head for values that range from 600 to 1200 m in this problem. A maximum head difference of 7.05 m was found, again a small percentage of the head value. This result is not surprising given the fixed head boundary conditions that "pin" the head values on the boundaries.

Noting that the temperature differences affect all the parameters equally throughout the grid, we can conclude that calibration is not affected significantly by temperature. The influence on flux is somewhat larger, which is not surprising given that the flux is inversely proportional to the viscosity. The two runs produced fluxes from the south face of the model of 462 kg/s and 637 kg/s, respectively. These differences are directly attributable to differences in viscosity.

These relatively small differences in head indicate that the temperature changes should not affect the calibration process significantly. We can conclude from this work that the flux values can be bounded by making flow runs with different uniform temperatures. We could also adjust the transport times described in this milestone by the simple viscosity-temperature relationship. The differences are small compared to other model uncertainties. The transport calculations

performed in Chapter 6 reflect the ambient temperature appropriate for the average depth of the simulation.

As a final note regarding temperature, for the regional-scale model calibration, the fitted parameters are hydraulic conductivities, which lump the density and viscosity with the intrinsic permeability. Thus, the flux values obtained with the regional model should be converted with the appropriate temperature values. The values assumed in the conversion were 20°C. Thus, the comparison given in the revised USGS milestone SP23NM3 is valid.

3.5 Updated Stratigraphic Framework Model

In Section 6.3, we describe some unwanted features in the geologic framework model of the current site-scale model (Figure 3-3) that make it difficult to produce accurate transport results in the vicinity of Yucca Mountain. These features do not significantly impact the calibration of the flow model but make transport simulations problematic. In parallel to producing this calibrated site-scale model, the USGS has been developing an updated geologic framework model (Figure 3-4) with more up-to-date geologic interpretation near Yucca Mountain. Our plan is to develop grids and calibrated flow solutions on this revised model early in FY98 and to use this revised flow model as the platform for performing radionuclide transport calculations.

The main difference between the two framework models is that the discretization of the revised-site SFM (Figure 3-4) is finer (250 m) than the older-site SFM (1500 m). This difference leads to smoother transitions between and more realistic representations of the hydrogeologic units. Additional data from the ISM framework model (Zelinski and Clayton, 1996) were incorporated into the 250-m framework model. This approach gives better resolution to the volcanic units. The representation of the upper volcanic confining unit (UVCU, Unit 14) is of importance due to its predominance in the control of the flow beneath the potential repository site. The UVCU appears primarily in the northern half of the 250-m framework model, with relatively isolated bodies in the southern part of the modeled area. The UVCU does not appear as a large

body in the central part of the model, as it does in the 1500-m framework model. It appears that the configuration of the UVCU in the 250-m framework model may produce the steep hydraulic gradients in the north, where it exists, and have a less dominant control on the flow field in the southern and central parts, where it does not exist.

With regard to transport, a revised flow model based on this geologic interpretation will correct the problems in the current version and allow realistic simulations from the potential repository to hypothetical accessible environment locations as far as 25 km from the site. In the meantime, we present results in Chapter 6 using a sub-site-scale model developed at Sandia National Laboratories (Ho et al., 1996) to perform predictions out to 5 km, and we pick up the simulations using the current site-scale model out to 20 km.

3.6 Correspondence of Site-Scale Units with RIB Stratigraphy

In this section, the hydrologic units defined in Chapter 3 and used in subsequent chapters are related to those in the RIB. This stratigraphy is identical to that used in the USGS flow model (Czarnecki et al., 1997) that forms the basis for transport modeling at the site scale. Table 3-2 shows this correspondence (Faunt, 1997, personal communication). The stratigraphy corresponds to that in the RIB database but is extended to cover the larger extent of the site-scale flow and transport model.

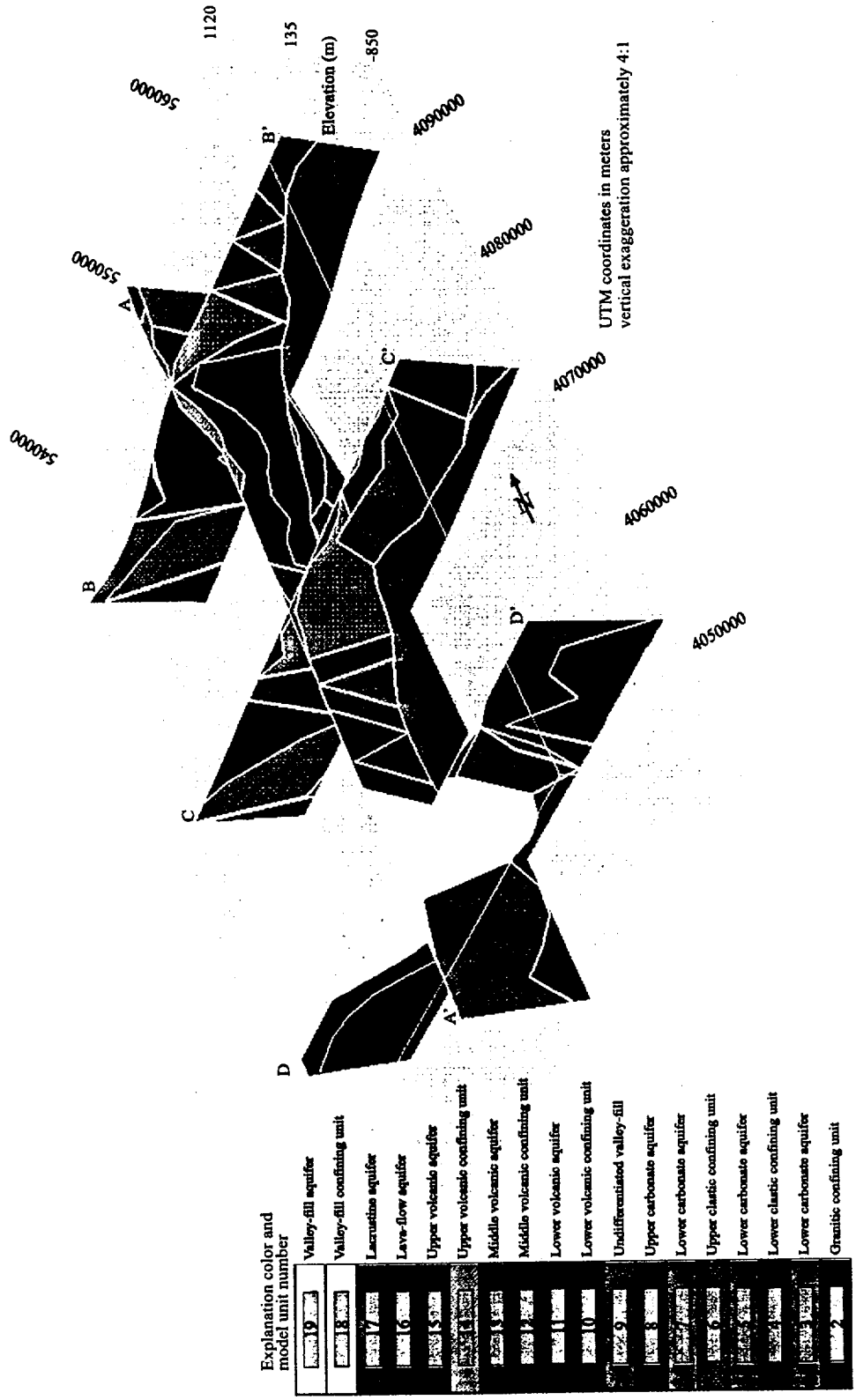

Figure 3-3. Fence diagram showing geologic cross sections for the current site-scale SZ model (from Czarnecki et al., 1997).

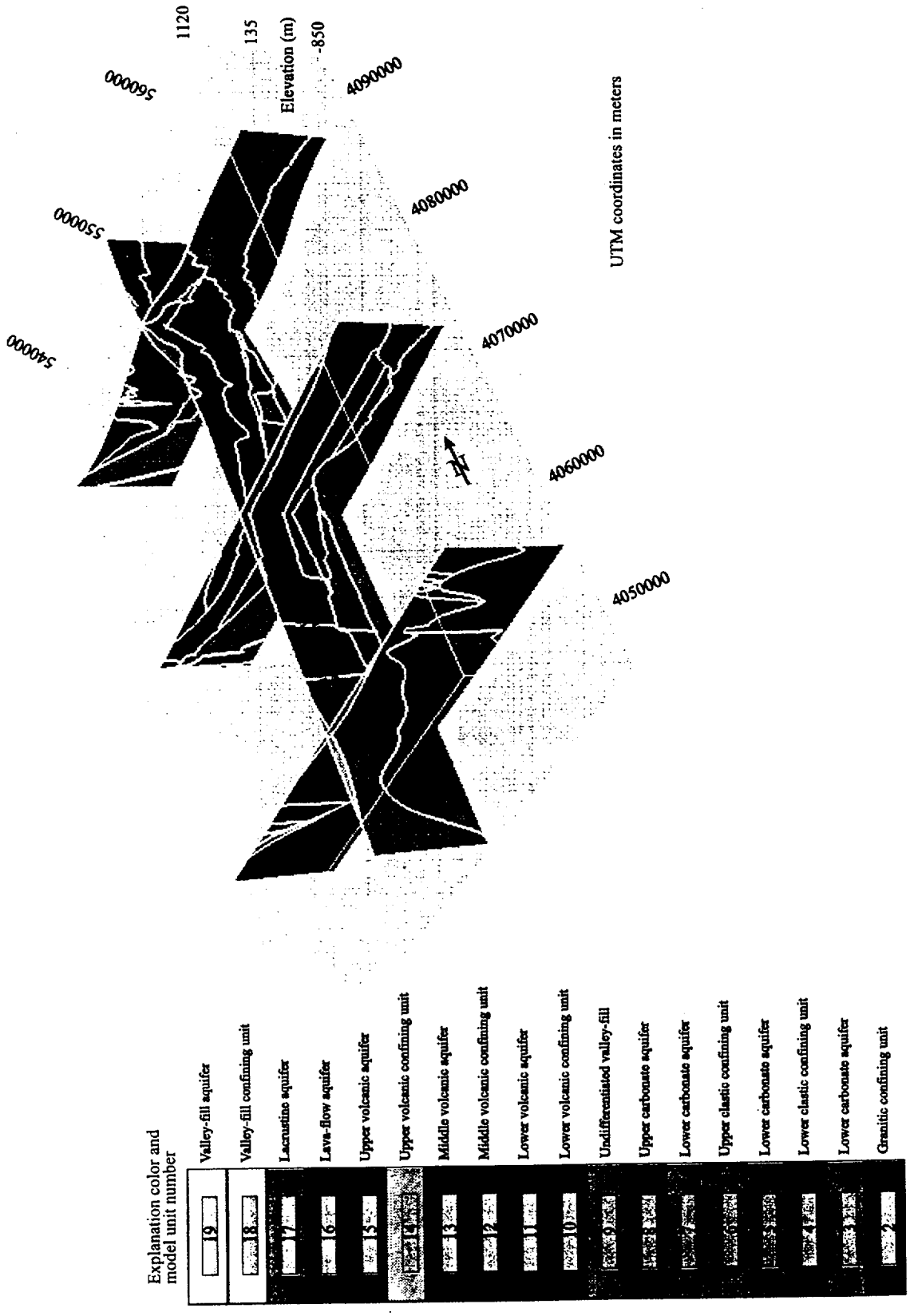

Figure 3-4. Fence diagram showing geologic cross sections for the updated site-scale SZ model.

Table 3-2. Comparison of ISM and Site-Scale Stratigraphy (provided by C. Faunt, 1997)

Site Saturated-Zone Hydro-geologic Unit	**Geologic Lithologic Stratigraphy (RIB item 1.1.2.1)**						**ISM2.0**
	Definition (Buesch,1996)	Group	Formation	Member	Zone	Subzone	
Valley-Fill Aquifer							
Valley-Fill Confining Unit							
Limestone Aquifer							
Lava-Flow Aquifer							
Upper Volcanic Aquifer	Timber Mountain Group	Tm					
Upper Volcanic Aquifer	Rainier Mesa Tuff		Tmr				44tmr
Upper Volcanic Aquifer	Paintbrush Group	Tp					
Upper Volcanic Aquifer	Post tuff unit "x" bedded tuff			Tpbt6			
Upper Volcanic Aquifer	Tuff unit "x"			Tpki (informal)			44tpk
Upper Volcanic Aquifer	Pre-tuff unit "x" bedded tuff			Tpbt5			44tpc
Upper Volcanic Aquifer	Tiva Canyon Tuff		Tpc				
Upper Volcanic Aquifer	Crystal-rich Member			Tpcr			
Upper Volcanic Aquifer	Vitric zone				Tpcrv		
Upper Volcanic Aquifer	Nonwelded subzone					Tpcrv3	
Upper Volcanic Aquifer	Moderately welded subzone					Tpcrv2	
Upper Volcanic Aquifer	Densely welded subzone					Tpcrv1	
Upper Volcanic Aquifer	Nonlithophysal zone				Tpcrn		
Upper Volcanic Aquifer	Subvitrophyre transition subzone					Tpcrn4	
Upper Volcanic Aquifer	Pumice-poor subzone					Tpcrn3	
Upper Volcanic Aquifer	Mixed pumice subzone					Tpcrn2	
Upper Volcanic Aquifer	Crystal transition subzone (not always present)					Tpcrn1	
Upper Volcanic Aquifer	Lithophysal zone				Tpcrl		

Upper Volcanic Aquifer	Crystal transition subzone (not always present)					Tpcrll	
Upper Volcanic Aquifer	Crystal-poor Member			Tpcp			
Upper Volcanic Aquifer	Upper lithophysal zone				Tpcpul		
Upper Volcanic Aquifer	Spherulite-rich subzone					Tpcpull	
Upper Volcanic Aquifer	Middle nonlithophysal zone				Tpcpmn		
Upper Volcanic Aquifer	Upper subzone					Tpcpmn3	
Upper Volcanic Aquifer	Lithophysal subzone					Tpcplnn2	
Upper Volcanic Aquifer	Lower subzone					Tpcpmn1	
Upper Volcanic Aquifer	Lower lithophysal zone				Tpcpll		
Upper Volcanic Aquifer	Hackly-fractured subzone					Tpcpllh	
Upper Volcanic Aquifer	Lower nonlithophysal zone				Tpcpln		
Upper Volcanic Aquifer	Hackly subzone					Tpcplnh	
Upper Volcanic Aquifer	Columnar subzone					Tpcplnc	
Upper Volcanic Aquifer	Vitric zone				Tpcpv		
Upper Volcanic Aquifer	Densely welded subzone					Tpcpv3	44tpcpv3
Upper Volcanic Aquifer	Moderately welded subzone					Tpcpv2	44tpcpv12
Upper Volcanic Aquifer	Nonwelded subzone					Tpcpv1	44tpcpv12
Upper Volcanic Aquifer	Pre-Tiva Canyon bedded tuff			Tpbt4			44tpbt4
Upper Volcanic Aquifer	Yucca Mountain Tuff		Tpy				44tpy
Upper Volcanic Aquifer	Pre-Yucca Mountain bedded tuff			Tpbt3			44tpbt3
Upper Volcanic Aquifer	Pah Canyon Tuff		Tpp				44tpp
Upper Volcanic Aquifer	Pre-Pah Canyon bedded tuff			Tpbt2			44tpbt2
Upper Volcanic Aquifer	Topopah Spring Tuff		Tpt				
Upper Volcanic Aquifer	Crystal-rich Member			Tptr			
Upper Volcanic Aquifer	Vitric zone				Tptrv		
Upper Volcanic Aquifer	Nonwelded subzone					Tptrv3	44tptrv23
Upper Volcanic Aquifer	Moderately welded subzone					Tptrv2	44tptrv23

Upper Volcanic Aquifer	Densely welded subzone					Tptrv1	44tptrv1
Upper Volcanic Aquifer	Nonlithophysal zone				Tptrn		44tptrn
Upper Volcanic Aquifer	Dense subzone					Tptrn3	
Upper Volcanic Aquifer	Vapor-phase corroded subzone					Tptrn2	
Upper Volcanic Aquifer	Crystal transition subzone (not always present)					Tptrn1	
Upper Volcanic Aquifer	Lithophysal zone				Tptrl		
Upper Volcanic Aquifer	Crystal transition subzone (not always present)					Tptrl1	44tptrl
Upper Volcanic Aquifer	Crystal-poor Member			Tptp			
Upper Volcanic Aquifer	Lithic-rich zone			Tptpf or Tptrf			44tptf
Upper Volcanic Aquifer	Upper lithophysal zone				Tptpul		44tptpul
Upper Volcanic Aquifer	Middle nonlithophysal zone				Tptpmn		44tptpmn
Upper Volcanic Aquifer	Nonlithophysal subzone					Tptpmn3	
Upper Volcanic Aquifer	Lithophysal-bearing subzone					Tptpmn2	
Upper Volcanic Aquifer	Nonlithophysal subzone					Tptpmn1	
Upper Volcanic Aquifer	Lower lithophysal zone				Tptpll		44tptpll
Upper Volcanic Aquifer	Lower nonlithophysal zone				Tptpln		44tptpln
Upper Volcanic Aquifer	Vitric zone				Tptpv		
Upper Volcanic Aquifer	Densely welded subzone					Tptpv3	44tptpv3
Upper Volcanic Aquifer	Moderately welded subzone					Tptpv2	44tptpv12
Upper Volcanic Aquifer	Nonwelded subzone					Tptpv1	44tptpv12
Upper Volcanic Aquifer	Pre-Topopah Spring bedded tuff			Tpbt1			44tpbt
Upper Volcanic Confining Unit	Calico Hills Formation		Ta				44tac
Upper Volcanic Confining Unit	Bedded tuff			Thtbt			44tacbt
Middle Volcanic Aquifer	Crater Flat Group	Tc					
Middle Volcanic Aquifer	Prow Pass		Tcp				44tcplnw, 44cpunw, 44tcpw

Middle Volcanic Aquifer	Bedded tuff			Tcpbt			44tcpbt
Middle Volcanic Aquifer	Bullfrog Tuff		Tcb				44tcblnw, 44tcbunw, 44tcbw
Middle Volcanic Aquifer	Bedded tuff			Tcbbt			44tcbbt
Middle Volcanic Aquifer	Tram Tuff		Tct				44tct
Middle Volcanic Aquifer	Bedded tuff			Tctbt			44tctbt
Middle Volcanic Aquifer	Lava and flow breccia (informal)			Tll			
Middle Volcanic Aquifer	Bedded tuff			Tllbt			
Middle Volcanic Aquifer	Lithic Ridge Tuff		Tr				
Middle Volcanic Aquifer	Bedded tuff			Tlrbt			
Middle Volcanic Aquifer	Lava and flow breccia (informal)			Tll2			
Middle Volcanic Aquifer	Bedded tuff			Tll2bt			
Middle Volcanic Aquifer	Lava and flow breccia (informal)			T113			
Middle Volcanic Aquifer	Bedded tuff			Tll3bt			
Middle Volcanic Aquifer	Older tuffs (informal)			Tt			
Middle Volcanic Aquifer	Unit a (informal)			Tta			
Middle Volcanic Aquifer	Unit b (informal)			Ttb			
Middle Volcanic Aquifer	Unit c (informal)			Ttc			
Middle Volcanic Aquifer	Sedimentary rocks and calcified tuff (informal)			Tca			
Middle Volcanic Aquifer	Tuff of Yucca Flat (informal)			Tyf			
Middle Volcanic Confining Unit							
Lower Volcanic Aquifer							
Lower Volcanic Confining Unit							
Undifferentiated Valley-Fill							

Upper Carbonate Aquifer							
Upper Clastic Confining Unit							
Lower Carbonate Aquifer	Lone Mountain Dolomite		Slm				paleozoic Grav (not used)
Lower Carbonate Aquifer	Roberts Mountain Formation		Srm				paleozoic Grav (not used)
Lower Clastic Confining Unit							
Granitic Confining Unit							

3.7 Conclusions

The flow models used in this report were provided by the USGS and Sandia National Laboratories. The USGS model used was the most recently calibrated model and includes a correction that results in reasonable flux values on the model boundaries. A comparison of flux values out of the site-scale model yielded values in good agreement with values predicted by the regional-scale model. For example, the calibrated site-scale model has a flux of 465 kg/s from the south face versus 323 kg/s over the same region for the regional model. This agreement is acceptable considering the compatibility issues raised in this chapter. Due to coarse sampling (1500 m), the region under the repository overpredicted travel times to the accessible environment. This problem was corrected in this report by using the finer-scale Sandia model described in Chapter 6 out to the periphery of that model and using the results as input to the site-scale model. In early FY98, we will use the newer USGS framework model, making this "piecing together" of models unnecessary.

Chapter 4 - Grid Generation and Grid Resolution Studies

4.1 Summary

Several three-dimensional grids were generated in support of the site-scale flow and transport modeling effort. Both structured and unstructured grids were developed, tested, and used for sensitivity analyses and flow calibration studies. Structured grids, commonly referred to as finite-difference grids, are easy to generate but their blocklike structure makes it difficult to represent complicated geometries with all but the finest grid resolution. Unstructured grids, like the common finite-element meshes, are more complicated and may consist of triangles and tetrahedrals. They can, however, represent complicated hydrostratigraphy and topography accurately at fairly low resolution. The hydrostratigraphy represented in the geologic model consists of multiple layers of contrasting fluid flow and transport properties. The grid-generation methods used in the present study allow the stratigraphy to be honored in numerical grids of different resolution so that comparison studies can be performed to test for grid quality and to determine the resolution required for flow and transport simulations. All mesh generation and manipulation is done with the GEOMESH/X3D toolkit (Gable et al., 1995, 1996; Trease et al., 1996).

A series of six structured grids of increasing resolution were used to compare the flow through the model domain to assess the point at which increasing resolution no longer influences the results. This process identifies the resolution required for an accurate simulation of the flow field. A similar study for two unstructured grids demonstrated that the coarser grid used for calibrating the flow model was sufficiently resolved for accuracy. Finally, this chapter reports on the development of a technique for selectively refining the numerical grid for transport calculations. The method uses the solute transport pathway determined on a coarse grid to identify regions of the model where increased grid resolution is required. The mesh-generation software refines the grid in those areas. After two or more successive applications of this process, the grid is finely resolved along the pathways of

solute plume movement, and numerical error associated with insufficient grid resolution is minimized. This technique is demonstrated in a simplified three-dimensional model, and the process is then described for the site-scale model grid. The main application of this technique will be for refining the revised site-scale model for transport calculations.

4.2 Software and Data QA Status

The FEHM code is used to perform all flow and transport calculations in this report. The code is qualified in accordance with Los Alamos quality-assurance (QA) requirements and is documented in several reports by Zyvoloski et al. (1992, 1996b–d). The QA status of the data used in this chapter is shown in Table 4-1.

Table 4-1. QA Status of Data used in this Chapter

REFERENCE	QA Status	DTN/ Assession Number	COMMENT
Czarnecki, J. B., et al. 1997. Preliminary three-dimensional finite-element groundwater flow model of the saturated zone, Yucca Mountain, Nevada. USGS YMP milestone number SP23NM3.	non-Q		
Clayton, R. W., et. al. 1997. ISM2.0: A 3-D geological framework and integrated site model of Yucca Mountain: Version ISM1.0, Doc ID B00000000-01717-5700-00004, Rev. 0, MOL. 19970122.0053. CRWMS M&O,	Q	MOL. 19970122.0053	By agreement with DOE and NRC, accepted as Q even though it uses some non-Q data.
Zelinski, W. P., and R. W. Clayton. 1996. A 3-D geological framework and integrated site model of Yucca Mountain: Version ISM1.0, Doc ID B00000000-01717-5700-00002, Rev. 1. CRWMS M&O.	non-Q		

4.3 Introduction

This chapter addresses the construction of computational grids that reflect complex geologic structure for saturated-zone flow and transport simulations. The importance of grids can be summarized with the following questions:

- What resolution is required to represent geology?
- What resolution is required to represent flow and transport processes?
- Can a grid be optimized to represent features and flow processes while keeping the size relatively small?
- If a flow model is calibrated on a coarse grid, is it calibrated on a fine grid?

These grids must accurately represent the geologic structure and be appropriate for numerically accurate simulations of flow and transport. That is, any error associated with numerical grid discretization must be constrained within specified truncation error tolerances. Understanding the quality of the grids and the effects of grid-related error is necessary for assessing the quality of the simulations and generating a defensible model.

The process of developing flow and transport models for the saturated-zone studies can be divided into three parts:

- Developing accurate conceptual models of the geology and hydrologic material properties.
- Building the grid and prescribing boundary and initial conditions.
- Applying the computational physics models of flow, heat transport, and chemical transport.

Geologic interpretation, stratigraphic model development, and material characterization are performed based on numerous field measurements. The stratigraphic model populated with hydrologic material properties then provides the basis for computational grid development. The ability of the numerical grid to represent the geologic complexity directly affects accuracy of the numerical model's approximation of the actual physical system's response.

GEOMESH/X3D (Gable et al., 1995, 1996; Trease et al., 1996) is a mesh-generation toolkit that can use the hydrostratigraphic model as input to create a numerical grid that represents accurately complex structures and stratigraphy such as faults, pinchouts, and layer truncations. As well as representing geologic structure, this software maintains and distributes physical and chemical attributes such as porosity, permeability, or percent zeolite. The process of populating the numerical grid with hydrologic and transport properties is described in Robinson et al.,1997.

The process of generating and populating numerical grids from geologic framework models is automated, thus making the entire process easy to implement with fewer user-induced errors. At any step in the process, greater numerical resolution can be added to a particular subregion, new boundary conditions can be prescribed, or new attributes can be incorporated.

The grid-quality control issues involved in this automated process cannot be over-emphasized. We believe that a system that uses only electronic processing of the hydrogeologic data is desirable for a defensible model during the licensing process because the interfaces can be qualified and metrics of goodness of representation can be established. These metrics would likely include a volume comparison between the project database hydrogeologic units and the model hydrogeologic units.

As part of our study, we are interested in analyzing how accurately grids of increasing resolution capture this complex structure and simulate flow. At what resolution is the geometry of the material distribution accurately represented with a structured grid in order to model fluid flow through the aquifer? Because higher grid resolution is more computational expensive, we can use this information to determine what the desired accuracy of the result is and at what resolution of grid that accuracy would be attained.

4.4 Saturated-Zone Unstructured Mesh from Stratamodel Geological Model

Software has been developed to automate the steps required to create a finite-element mesh for flow and transport calculations from a geological framework model.

The steps required to create a grid are:

- Convert Stratamodel Stratigraphic Framework Model (SFM) provided by USGS to hexahedral finite-element grid.
- Remove zero volume elements from data structure.
- Remove elements with vertical height less than one meter.
- Convert hexahedral elements to tetrahedral elements.
- Add the points defining the potentiometric surface (surface provided by the USGS).
- Add nodes with specified *xyz* location for measured well-head calibration.
- Add nodes above and below well-head calibration nodes to enhance grid quality.
- Add buffer zones above potentiometric surface and below bottom boundary.
- Assign material values to all nodes.
- Optimize the grid connectivity to insure positive finite-element coefficients.
- Calculate Voronoi control volumes.
- Output node coordinates, node connectivity, nodal volumes, and material and boundary lists.

All file conversion, gridding, node distribution, property interpolation, quality checking, and output is carried out within a single integrated gridding tool kit. This approach insures that the steps taken are reproducible and traceable and modifications to any step in the gridding process can be done without a great deal of labor.

4.5 Grid Generation and Property Interpolation

Generation of grids and interpolation of properties from the hydrostratigraphic model onto the numerical grids is performed with GEOMESH/X3D. GEOMESH/X3D is also used for comparing results from different grids, each having different resolution or grid structure. Interpolation with GEOMESH/X3D allows for the superposition on mesh A of the attributes (material number, pressure, saturation, concentration, etc.) belonging to mesh B. This utility is

useful when refining a mesh or when comparing meshes of different resolution. The meshes should generally be of the same volume but do not have to coincide exactly. They do not have to have the same discretization, resolution, or element type. Either mesh can be structured or unstructured. For interpolation, a node of mesh A is first located within an element of mesh B. The attributes of the nodes defining the element in mesh B are then linearly interpolated to the node in mesh A. Output of mesh A from GEOMESH then contains the new attribute values associated with each node. If desired, the mesh-A node is also assigned the material number of the mesh-B element. Elements of mesh A can then be assigned material numbers based on the nodal material numbers that were interpolated from mesh B.

The saturated-zone model domain selected for this grid resolution study is defined by Nevada State Coordinates of 533,340 m to 563,340 m in an east-west direction, 4,046,782 m to 4,091,782 m in the north-south direction, and –754 to 1332 m vertically above sea level. Nineteen materials are assumed located within this volume as shown in Figure 4-1.

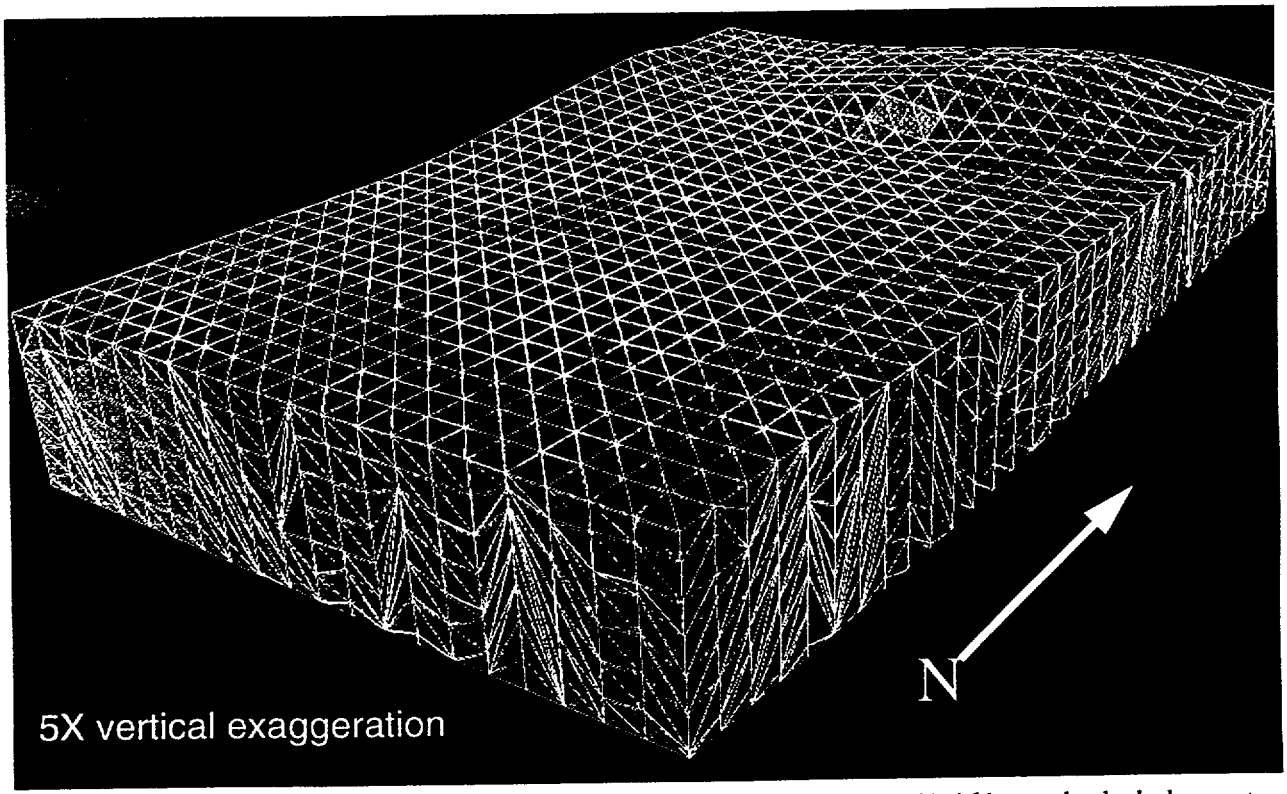

Figure 4-1. Saturated-zone computational grid with 9,279 nodes and 51,461 tetrahedral elements. The upper and lower buffer zones have been removed for visualization.

The permeability of the various units is listed in Table 4-2.

Table 4-2. Permeability and Volume of the Geologic Materials

Material number	Name	Permeability (m^2)
2	Granites	3.5e-14
3	Lower carbonate aquifer	3.3e-12
4	Quartzite confining unit	2.0e-15
5	Lower carbonate aquifer	3.3e-12
6	Eleana confining unit	5.5e-19
7	Lower carbonate aquifer	3.3e-12
8	Upper carbonate aquifer	6.7e-13
9	Leaky confining unit	2.9e-14
10	Lower volcanic confining unit	1.0e-16
11	Lower volcanic aquifer	5.0e-13
12	Middle volcanic confining unit	1.9e-16
13	Middle volcanic aquifer	5.9e-15
14	Upper volcanic confining unit	1.0e-18
15	Upper volcanic aquifer	5.9e-15
16	Basalts	4.5e-14
17	T limestone confining unit	1.0e-14
18	Playa deposits	3.0e-16
19	Alluvium	6.6e-14

Although a calibrated model must have appropriate heads at each inlet and outflow boundary, to test the resolution of the various grids used, the actual pressure differential between the north and south is not important. For simplicity, a pressure difference of 15 MPa is used for all simulations in this grid resolution study. The isothermal model is run to steady state and the flow out of the model is compared for each grid. The effect of gravity on the fluid flow is ignored for this numerical experiment. The problem was designed to study the errors made only in the representation on the hydrostratigraphy. This was achieved by specifying pressures on the north and south faces of the grid. Thus, the solution is a linear variation in pressure with a corresponding constant flux. Tests with homogeneous meshes confirmed this result. The differences in reported fluxes are a result only of representation errors of the hydrogeologic units. The outlet flux was

chosen as the parameter to compare because this parameter is likely to be a primary factor in assessing radionuclide transport to the accessible environment.

4.6 Structured Grid Results

Six structured grids were constructed using GEOMESH, and hydrostratigraphic material properties are interpolated onto them. The number of nodes in the x, y, and z directions are chosen so that the nodes in the z-direction are equal to the number in the x-direction. The nodes are connected into tetrahedral elements. The grid details are shown in Table 4-3. For visual comparison, the stratigraphic model was given in Figure 3-3, the material distribution for grid 5 is shown in Figure 4-2.

Table 4-3. Grid Resolution Details

Grid number	Total number of nodes	Number of nodes, x & z	Number of nodes, y	Spacing of nodes, x & y (m)	Spacing of nodes, z (m)
1	96	4	6	3333	696
2	175	5	7	7500	521
3	1053	9	13	3750	260
4	7225	17	25	1875	130
5	23125	25	37	1250	87
6	40500	30	45	1000	70

The interpolation algorithms work by determining the material number of the element of the original grid that the structured-grid node is located within. Any nodes from the structured grid that fall outside the original grid geometry are assigned a material number of 20. Because the nodal locations are different for each of the six grids constructed, the volumes of the resulting materials change from grid to grid. The finer the structured mesh gets, the more closely the volumes of the materials match those of the stratigraphic model (Figure 4-3). It is also evident from Figure 4-3 that materials with large volumes are less affected by low-resolution grids than small volume units.

Each of the six grids is used to model flow through the saturated zone. A pressure difference of 15 MPa was applied on the north and south boundaries. The resulting fluid flow out

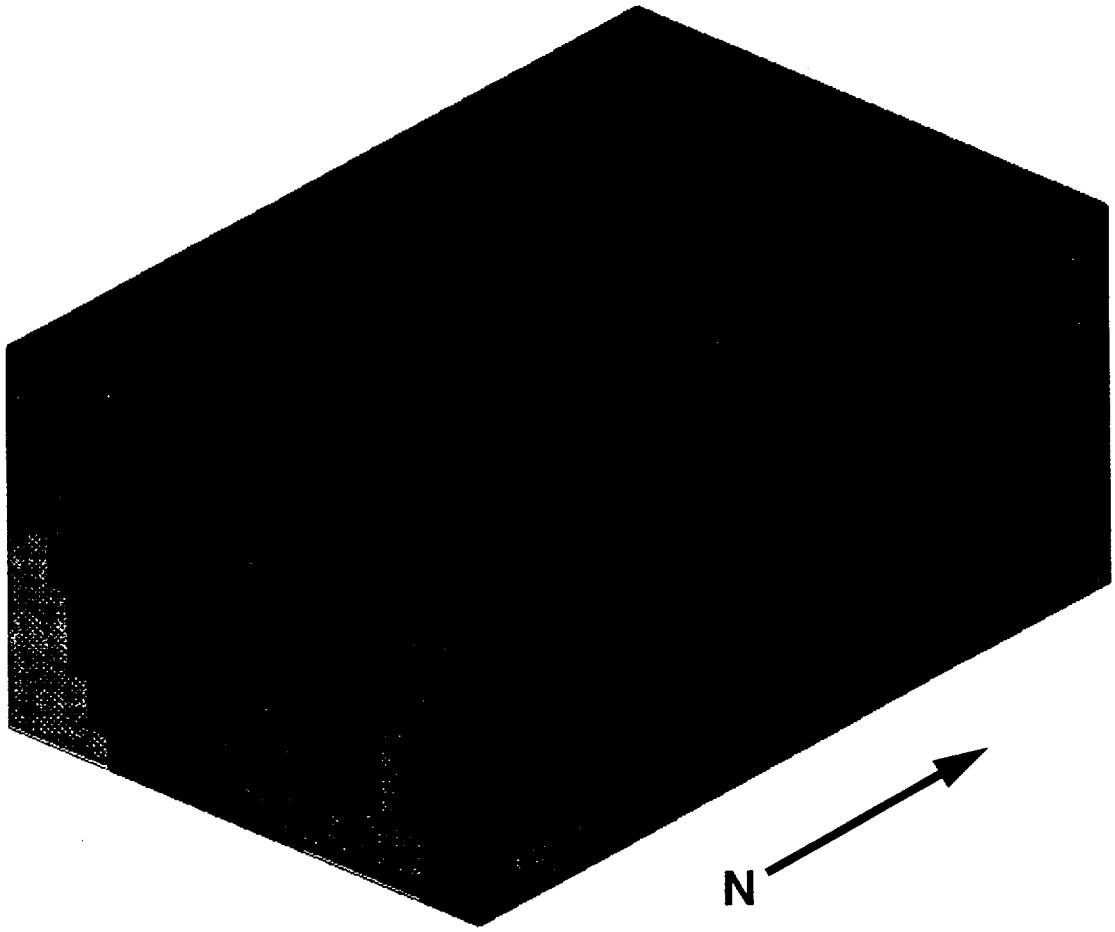

Figure 4-2. Grid 5 of Table 4-3 with material properties interpolated from the geologic framework model.

of the model is used to compare the effectiveness of each grid in representing the effects of the hydrostratigraphy on flow behavior. This flow was obtained by summing the outflow at the south boundary of the model. The resulting flow from each grid is shown in Figure 4-4. The curve shows asymptotic behavior at higher resolution. Because higher grid resolution is more expensive,

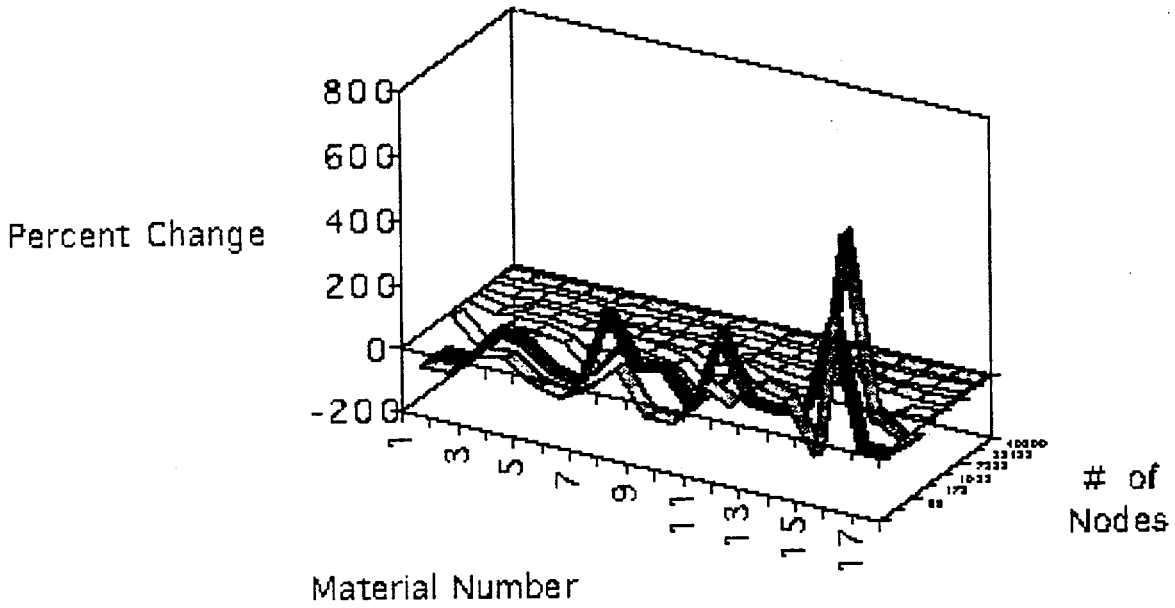

Figure 4-3. The percent change of each material's volume compared to the original material volume is affected by the grid resolution.

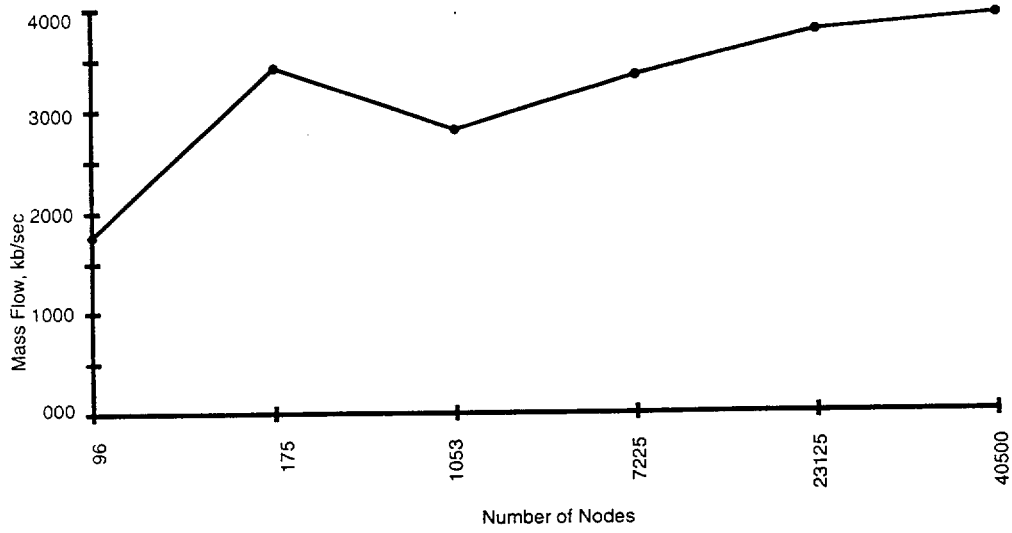

Figure 4-4. Flow out of models represented by structured grids. Increasing resolution results in convergence of mass flux towards an asymtotic value.

we can use this type of analysis to determine what the desired accuracy is and at what resolution that accuracy would be attained.

The results of the flux changes with grid resolution can be more easily understood in terms of average grid spacing. The range of grid spacings in the vertical direction range from 696 m to 70 m. The results of this study suggest that for saturated-zone computations, 100-m vertical grid resolution may be sufficient if structured or finite-difference gridding is used. This resolution is a finer grid than is commonly used in saturated-zone simulations of Yucca Mountain. In Section 4.7 we present runs with unstructured-grid representations to determine the resolution necessary for unstructured grids. It is anticipated that the restrictions of grid resolution will be somewhat relaxed if the stratigraphy is captured directly in the unstructured numerical grid. However, note also that this grid resolution study was conducted using total outflow water flux. If a criterion based on radionuclide transport was used, the result would most likely imply the need for higher grid resolution due to the nature of simulating transport using the advection-dispersion equation. Selective grid refinement in the region near the repository and close to the water table in the pathways to the accessible environment will be required for radionuclide transport. Future studies will shed additional light on this requirement.

4.7 Unstructured Grid Studies

As stated in Section 4.6, it is anticipated that the unstructured grid would produce closer flux agreement between grids of different resolution than the structured study mentioned above. To investigate this hypothesis, a finer-resolution model was generated by refining the geological model SFM. This model has approximately 2X resolution in the x, y, and z directions. The finer model is shown in Figure 4-5. The volume of each stratigraphic unit is identical to the lower-resolution model. The boundary conditions used are the same as described in Section 4.6—that is, a 15 MPa difference between the north and south faces with no flow on the top, bottom, east, and west. Again, we compare the flux flowing out of the south face. The results were 3290 kg/s for

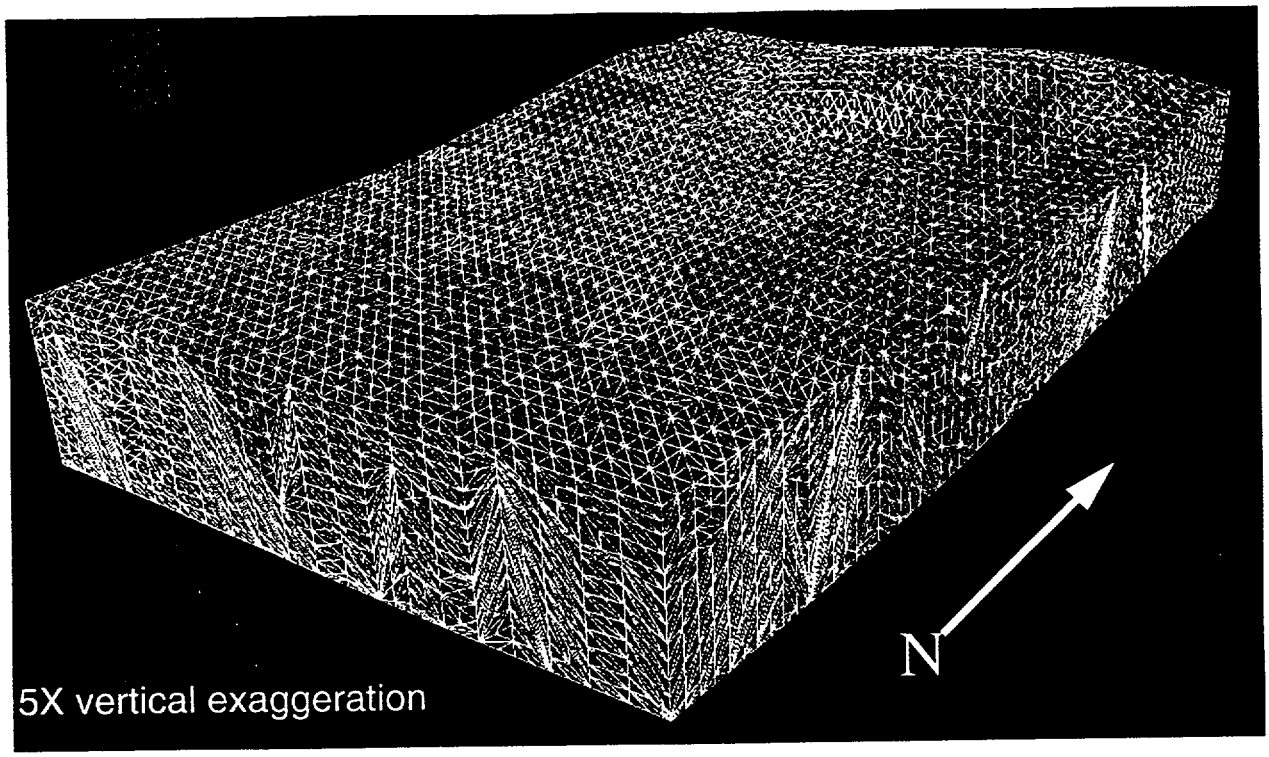

Figure 4-5. High-resolution grid with 49,895 nodes and 293,409 tetrahedral elements.

the lower-resolution model (9279 nodes) and 3760 kg/s for the higher-resolution model (49,895 nodes). The flow rates differ by about twelve percent. The results indicate that the flow calibration with the lower-resolution model is sufficient but some caution is warranted. Time constraints precluded additional resolution studies. As indicated in Section 4.6, transport simulations would require additional resolution. These studies do point to a need to systematically study grid refinement and its relation to both flow and transport.

4.8 Grid Refinement Around Plumes

To adequately model contaminant transport through porous media, a computational grid will require refinement beyond that required for flow modeling. This requirement is true of the grid used for USGS/LANL site-scale saturated-zone flow simulations of the regional aquifer beneath Yucca Mountain (Czarnecki et al., 1997). We have developed an approach for grid refinement that refines only that part of the grid where most contaminant migration occurs, thus

minimizing the number of nodes added to the grid to assure an accurate transport solution. The refinement technique uses the results of a transport solution computed on a grid that is expected to be too coarse for an accurate transport solution. The preliminary coarse grid is then refined in the region where most contaminant migration occurs (e.g., within a specified isoconcentration surface). The flow and transport solution is recalculated on the refined grid. This grid may then be refined again within an isoconcentration surface that is generally of lower concentration than used for the initial refinement. Refinement is complete when the breakthrough curves computed at some compliance point no longer vary within a specified tolerance level. This approach is a form of adaptive mesh refinement that uses the problem solution to guide the refinement process. The technique, which uses the GEOMESH/X3D grid-generation system, was first tested on a rectangular grid with a single porous medium. This case is discussed, as it is useful in explaining the refinement methodology. The technique, tested below, will be employed in FY98 to the 250-m sampled SFM currently being developed by the USGS.

4.8.1 Single-material grid

In this section, we discuss the grid-refinement technique using the single-material grid as an example. We start with a uniform, single-material grid of 5793 nodes and 36,864 tetrahedral elements. This grid has the same external dimensions as the desired site-scale grid. A pressure gradient, of the same magnitude as the site-scale saturated-zone model, is applied across the north and south boundaries to create a steady flow field. Then, contaminant of uniform concentration is introduced into a few upstream nodes that are meant to represent the entry region of radionuclide migrating from the potential repository through the vadose zone and into the aquifer. The transport calculation is run to steady state, resulting in a plume that identifies all nodes where contaminant travels through the grid. Figure 4-6 shows the resulting plume for this coarse uniform grid.

The coarse grid was then refined within an isoconcentration surface of $C = 0.1$. The steady flow and transport solutions were recomputed on the resulting grid. A second level of refinement was completed within the $C = 0.05$ isoconcentration surface, and again, the flow and transport solutions were updated. Figure 4-7 shows the resulting 28,511-node grid after two levels of

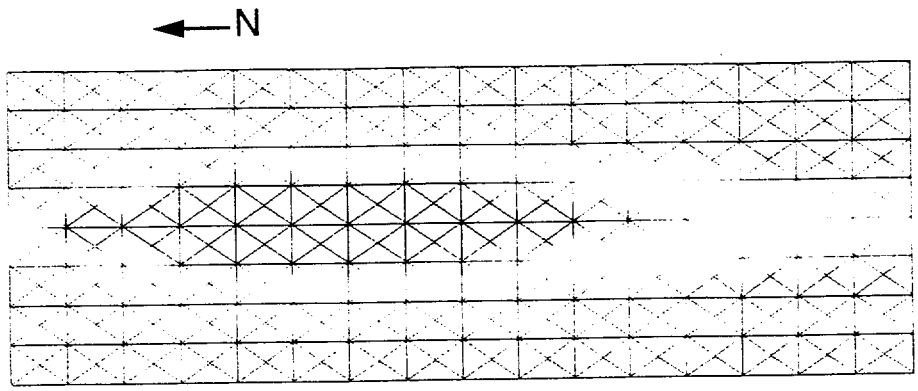

Figure 4-6. Plan view of steady-state transport solution on the coarse, single-material grid.

refinement, first at $C = 0.1$ and then at $C = 0.05$. The top view shows that the plume primarily travels in the direction of flow with little transverse spreading for this single-material case. Approximately 25% of the volume has undergone two levels of refinement, and an additional 25% of the grid that surrounds the center has undergone one level of refinement. The outer 50% of the grid is unchanged because the plume does not migrate to that region of the domain. The side view shows that most of the vertical refinement occurs near the surface even at the downstream boundary. Because this process is experimental, several other refined grids were generated using this same technique with differing isoconcentration surfaces. This approach allowed optimization of the concentration criteria.

A criterion is needed to determine when the grid is adequately refined. We have chosen to look for convergence in the breakthrough curve at a downstream compliance point. Figure 4-7 shows the breakthrough monitoring location, which is the uppermost, central node of the grid at the downstream boundary. We found that the original constant-concentration source used for grid refinement results in different solute mass-flux input rates with the different grids. Therefore, transport solutions were rerun with the various grids using constant tracer flux so that each

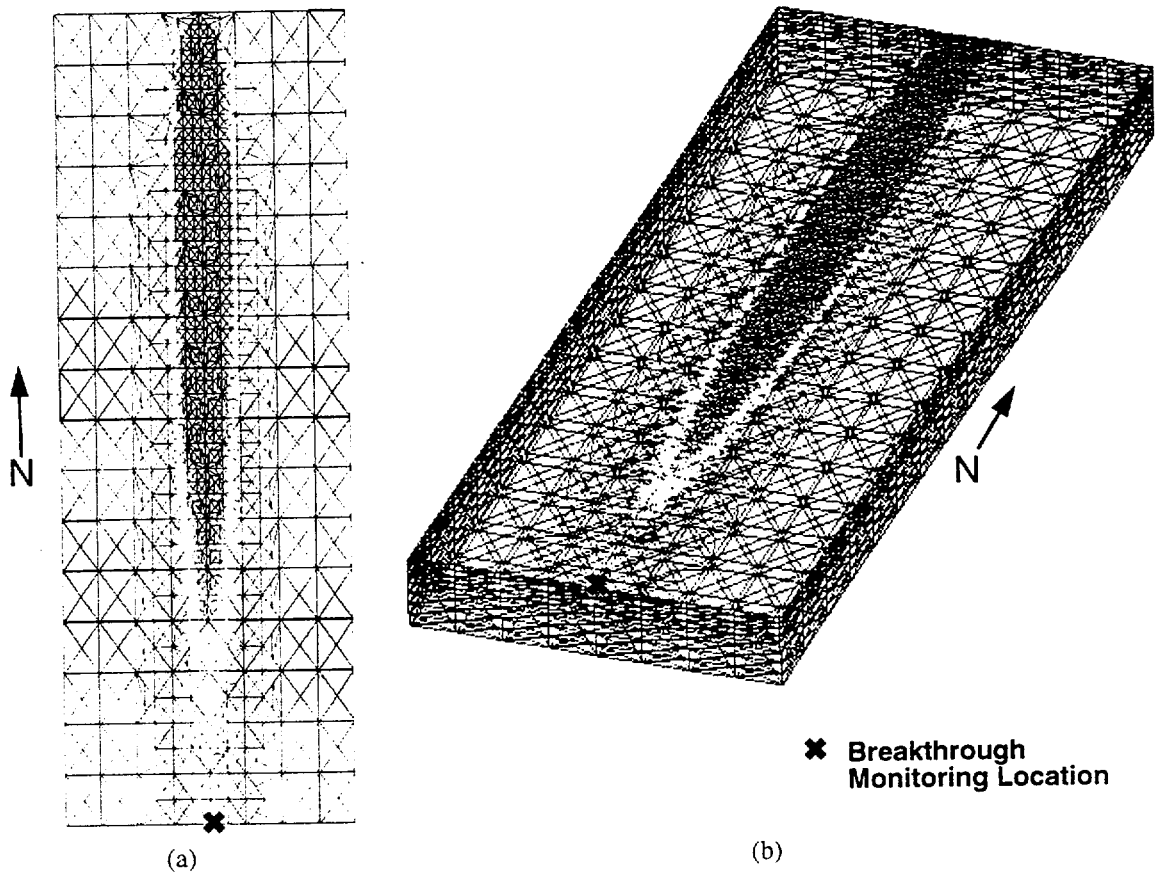

Figure 4-7. Single-material grid after two levels of refinement within isoconcentration surfaces of 0.1 and 0.05 with both (a) plan view and (b) perspective view.

simulation would receive the same mass, and the breakthrough curves could then be compared. Figure 4-8 shows breakthrough curves for several of the grids with the legend indicating the number of times the grid was refined (once or twice) and the isoconcentration surfaces used. As the grid is refined, breakthrough to the monitoring point advances slightly in time and the steady-state breakthrough concentration generally increases. This result occurs because the plume exhibits less numerical dispersion around its centerline and with depth. There is little difference between the solutions for the grids with 28,511 (0.1, 0.5) and 57,450 (0.05, 0.01) nodes indicating that the 28,511-node grid is adequately refined.

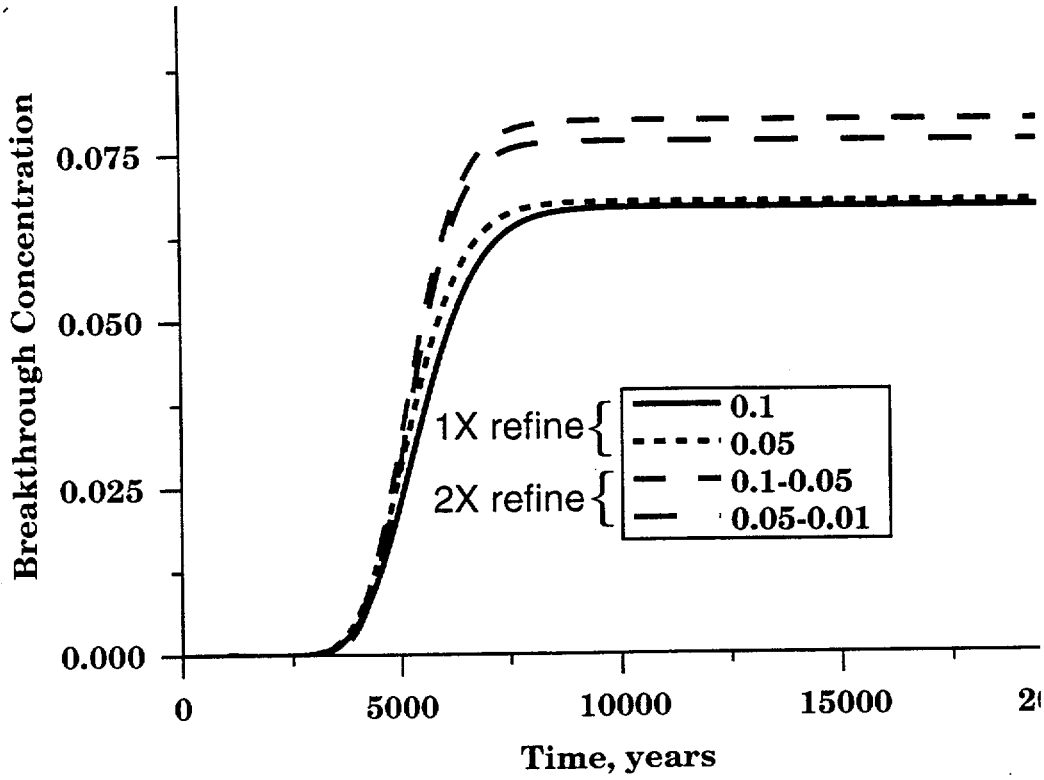

Figure 4-8. Breakthrough curves for various refinement levels of the single-material grid. Isoconcentration levels used to define refinement zone are given in the legend.

4.8.2 Multiple-material grid.

Future work will apply the refinement technique discussed above to the USGS/Los Alamos multiple-material saturated-zone model. Refinement will be based on the concentration of a steady plume generated with the calibrated flow field. Nodes added during refinement are assigned material properties based on the original Stratigraphic Framework Model discussed previously. The original nodes remain in the grid and retain their material properties. Refinement of the USGS/Los Alamos model was not pursued for this year's study. The coarse 1500-m spacing of the current stratigraphic framework model (SFM) is inadequately refined to justify refinement for transport simulations. An updated SFM with 250-m spacing will be incorporated in future work (see Sections 3.5 and 6.5). This refined SFM has adequate stratigraphic information to work ideally with the concentration adaptive mesh refinement technique.

4.9 Conclusions

Grid resolution was found to be a critical issue for both flow and transport. The ability to resolve heterogeneous geologic units was a function of grid resolution. Grid-resolution studies were carried out with both unstructured and structured grids. It was found that the USGS-calibrated flow model produced fluxes that changed little by resolving the grid and was thus deemed of sufficient resolution for flow simulation. A new method was described to locally resolve grids for transport simulations. The main application of this technique will be for refining the revised site-scale model for transport calculations.

Chapter 5 - Saturated Zone Conceptual Model for Radionuclide Transport

5.1 Summary

The site-scale groundwater flow model provides the hydrologic framework for determining the direction and rate of movement of radionuclides reaching the saturated zone beneath Yucca Mountain. In addition to flow issues, the migration of radionuclides to the accessible environment depends on transport processes and parameters distinct from the flow model itself. This chapter develops a conceptual model for transport that includes advective transport of radionuclides, dispersion, diffusion of radionuclides from fractures into the rock matrix, and sorption. Within the fractured tuffs, the migration of radionuclides is expected to be primarily through regions with higher bulk fracture permeability. Flow within individual joints probably occurs through channels, rather than as sheet flow through parallel-plate fractures. At more distant downstream locations, the migration is likely to be through alluvium, and a model for flow and transport through a porous continuum, rather than a fractured rock, is likely to apply.

For transport in porous, fractured tuff, radionuclides can escape the fractures by diffusion into the rock matrix. This process is a significant retardation mechanism that is likely to provide a benefit to performance. There have been several theoretical, laboratory, and field studies pointing to the validity of matrix-diffusion models. Of greatest relevance are the interwell tracer experiments at the C-Wells (Reimus and Turin, 1997) and the recently reported Nevada Test Site experiment of Waddell (1997). Both of these experiments used tracers with different diffusion coefficients to investigate whether differences in breakthrough curves could be detected in accordance with matrix-diffusion model predictions. The results of both tests point to the validity of the matrix-diffusion model for transport through fractured tuffs.

The degree of matrix diffusion detected in field tracer tests is small due to the short time scales in forced-gradient transport tests compared to transport in groundwater under natural

conditions. A theory is developed to estimate the impact of matrix diffusion on radionuclide migration in the saturated zone away from Yucca Mountain. We show that transport can be approximated using an effective transport porosity that, in general, falls between the fracture porosity and the porosity of the surrounding rock matrix. The key factors controlling this effective porosity are the groundwater flow velocity, travel distance, matrix diffusion coefficient, and mean spacing between flowing fractures. For transport in the saturated zone, effective porosities are apt to be much larger than the fracture porosity and, under some circumstances, approaching the matrix porosity. This leads to radionuclide travel times on the order of thousands of years compared to times on the order of one year if radionuclides are confined to the fractures. The matrix-diffusion model is shown to be consistent with ^{14}C ages measured for saturated-zone fluids, although the data do not rule out some differences in concentration between fracture and matrix fluids. A possible exception to the result of travel times in the thousands of years is colloid-facilitated transport of plutonium. This possibility is addressed with a mathematical model developed in this chapter that includes sorption to mobile colloids.

Dispersion is caused by heterogeneities at all scales from the pore scale to the scale of the thickness of individual strata and the length of structural features such as faults. The resulting spreading of radionuclides is important to performance and must be captured in transport models. Only the largest heterogeneities are represented explicitly in the site-scale model; all dispersion caused by smaller-scale features must be represented through the use of a dispersion model. Numerous groundwater transport studies have been conducted at a variety of scales, and the results are compiled using the dispersivity as the correlating parameter. It is well-known that dispersivity increases with the scale, or distance, of transport of a solute. The only site-specific data comes from the C-Wells reactive tracer experiment of Reimus and Turin (1997) and accompanying tracer tests carried out by the USGS at the C-Wells. These experiments yielded estimated dispersivity values that fall in the range of uncertainty of correlations to data collected and compiled at many sites. This result provides credibility that the dispersivity values used in the field simulations are appropriate.

5.2 Software and Data QA Status

The FEHM code is used to perform all flow and transport calculations in this report. The code is qualified in accordance with Los Alamos quality-assurance (QA) requirements and is documented in several reports by Zyvoloski et al. (1992, 1996a, 1996b). The QA status of the data used in this report is shown in Table 5-1.

Table 5-1. QA Status of Data used in this Chapter

REFERENCE	QA Status	DTN	COMMENT
Triay, I. R., et al. 1997. Summary report geochemistry/transport laboratory tests. Los Alamos National Laboratory milestone report SP23QM3.	Q	LAIT831341DQ97.003	
Stock, J. M., et al. 1984. Report on televiewer log and stress measurements in core hole USW G-2, Nevada Test Site, October–November, 1982. USGS open file report 84-172.	Non-Q		
Benson, L. V., et al. 1983. Chemical composition of groundwater and the location of permeable zones in the Yucca Mountain area. Nevada. USGS open file report 83-854.	Non-Q		

5.3 Introduction

The saturated-zone flow modeling performed for the Yucca Mountain Project has focused on the key controlling factors influencing the measured head distributions at the site. A summary of these conceptual models and numerical implementations of these models is presented in Czarnecki et al. (1997). In the present study, we are concerned with the transport of radionuclides in the saturated zone, which in addition to flow issues, requires that processes specific to the migration of solutes be considered. In this chapter, we present a conceptual model for transport

in fractured porous media that includes dispersion, interaction of radionuclides with the porous rock matrix, and sorption.

This chapter is organized as follows. We first review the relevant small-scale flow processes that will influence transport, focusing on fracture flow processes likely to influence radionuclide movement. We then outline a simplified matrix-diffusion model, describe the mathematics of the model, and perform simulations designed to assess the amount of matrix diffusion likely to be present in saturated-zone transport under natural conditions.

5.4 Fluid Flow in Fractures

The hydrologic evidence to date strongly supports the model of fluid flow within fractures in the moderately to densely welded tuffs of the saturated zone (e.g., Waddell et al., 1984; Whitfield et al., 1985). First, as expected, the hydraulic conductivities measured for core samples in the laboratory are orders of magnitude higher when the sample is fractured (Peters et al., 1984). Also, there is generally a positive correlation between fractures identified using acoustic televiewer or borehole television tools and the zones of high transmissivity. Evidence of this conclusion is shown in Figure 3 of Erickson and Waddell (1985).

Because the role of fractures is so important to the hydrology in the saturated zone, the permeability distribution and principal flow directions depend strongly on the spatial distribution and orientations of fractures. Erickson and Waddell's televiewer log data show 83.1 percent of the fractures having a strike direction between N 10°W and N 55°E, with most steeply dipping at angles greater than 60°. Karasaki and Galloway (1990) point out that fractures oriented perpendicular to the least principal stress direction of N 60–65°W (Stock and Healy, 1988) should be more open and thus be more permeable. Karasaki et al. (1990), in an attempt to correlate the C-Wells fracture data with transmissivity measurements, tentatively conclude that the regions of high transmissivity in the C-Wells correlate with fractures of this general orientation, with the steeply dipping fractures contributing most to the transmissivity.

To quantify this analysis, we may compare *in situ* stress measurements at Yucca Mountain with the laboratory data of the effective hydraulic aperture as a function of effective stress. Stock et al. (1984) report results of hydraulic-fracturing experiments in G-2 at 1026 m (in the Prow Pass Tuff) indicating a minimum horizontal principal stress S_h of 111 bar (with a N 60°W orientation), a maximum horizontal principal stress of 156 bar, and a vertical stress of 203 bar. Given a pore pressure of about 40 bar at this depth, the effective pressures (S - P) are P_h = 71 bar, P_H = 116 bar, and P_v = 163 bar.

Typical curves of effective hydraulic aperture versus effective pressure were reported by Peters et al. (1984). In the natural groundwater flow state, all fractures, regardless of orientation, will have effective pressure between P_h and P_v, or 71 to 163 bar. In this range, the laboratory tests of Peters et al. (1984) show a relatively minor effect of effective pressure on hydraulic aperture, at least compared with other uncertainties. Thus, it appears that the spatial distribution of fractures (densities and interconnectivities) is more important in determining the hydraulic conductivity ellipsoid than the effect of the stress field on the apertures of individual joints. However, pressure testing that lowers the effective pressure in a joint significantly will result in increased hydraulic apertures and erroneous estimates of the transmissivity. In fact, Stock et al. (1984) point out that, in some wells drilled with mud, the weight of the fluid column exceeded the minimum horizontal stress, probably resulting in induced hydraulic fracturing during drilling or the opening of favorably oriented preexisting joints. This possibility may also be true of some slug tests.

Even though we may make the simplifying assumption that, from a hydrologic standpoint, all joints are under similar effective stresses, the role of *in situ* stresses is nonetheless an important controlling factor governing the nature of fluid flow within a fracture. Numerical simulation studies (Brown, 1987) suggest that the nearly horizontal portion of the aperture versus effective pressure curves corresponds to larger contact areas of the two faces of the fracture. For transport, the result is a propensity of fluid and solute to travel preferentially along channels in which the

apertures are largest. Thus, for flow within fractures in the saturated zone, a channel flow model or a fracture flow model recognizing and accounting for flow channels is necessary.

5.5 Radionuclide Transport Conceptual Model Development

Given the complex geohydrologic setting, the most appropriate approach is to construct a plausible conceptual transport model that describes the relevant processes in the saturated zone. This model, along with its relatively straightforward mathematical representation, will allow us to identify the areas of uncertainty that are necessary to explore and incorporate into the site-scale model. It will be shown that the radionuclide transport times could be several orders of magnitude larger than the transport times computed assuming the fluid velocity within the fractures is the effective radionuclide migration velocity. This implies that the saturated zone could be a significant barrier to radionuclide migration. Therefore, field tests such as those at the C-Wells have been designed and carried out to validate the model (Robinson, 1994; Reimus and Turin, 1997).

5.5.1 Summary of Conceptual Model

Summarizing the discussion of fluid flow behavior given above, our saturated-zone fluid-flow model into which transport submodels are built is outlined below in narrative form.

- Radionuclides enter the saturated zone via the fluid percolating through the unsaturated rock above the water table. The exact nature of this transport is not expected to exert a great effect on the subsequent saturated-zone model, and thus, the saturated-zone transport model can be developed independently from a transport model for the vadose zone, which acts as a boundary condition for the saturated-zone model. Of course, for detailed predictions of radionuclide migration, the spatial and temporal distributions of the input from the unsaturated zone are important.
- Flow occurs within the highly fractured portions of the tuffs near the water table. There is probably not a continuous zone of high permeability to the accessible environment. Assuming

there is not, then the low-permeability regions will effectively act as large-scale heterogeneities that give rise to large-scale macroscopic dispersion due to the tortuous nature of flow over the scale of hundreds of meters to kilometers.

- Although the vertical matrix permeability is assumed to be small over the length scale of several hundreds of meters, within a fractured region, vertical permeabilities should be as large as the horizontal permeabilities. Thus, the radionuclide will spread vertically and be present within the entire thickness of a fractured zone. The thicknesses of these fractured zones are difficult to estimate from the present data. However, the extent of fracturing correlates reasonably well with the degree of welding, which is one of the criteria used to define the submembers within a lithologic unit. Therefore, it seems reasonable to assume that the heights of the fracture zones are on the order of the thicknesses of the individual lithologic members, namely 100 to 200 m. This possibility is in contrast to flow zones detected in individual boreholes, where measurements reflect the intersection of specific fractures with the well.

- Fluid flow occurs within the fractures with stagnant fluid residing in the rock matrix blocks. All fractures have large contact areas due to the *in situ* stresses exerted on them at these depths. The conductivity of an individual fracture is probably not a strong function of its orientation because all are on the flat portion of the aperture versus effective-pressure curves. Therefore, the magnitude and direction of the components of the hydraulic conductivity tensor should be controlled by the distribution of joints of various orientations. Fractures detected from geophysical logs are generally oriented in a north-south direction and are within 30° of vertical.

- Flow within individual joints probably occurs within channels. The fluid travels preferentially within regions of large apertures with large sections of the fracture surface containing stagnant fluid or no fluid where the faces are in contact.

- The surrounding matrix material conducts no fluid under natural groundwater flow conditions but is physically connected to the fracture fluid through the pore network. Fluid is stored in this pore space and is important to radionuclide migration (see below). The matrix porosities

of interest are those of the rock within the fractured regions. Fractures are generally found within the moderately to densely welded tuffs, so the range of matrix porosities of these tuffs (0.06 to 0.09 for densely welded and 0.11 to 0.28 for moderately welded) more accurately reflect the fluid storage of interest rather than the generally wider ranges of values found within a specific lithologic member.

5.5.2 Matrix Diffusion - Laboratory and Field Evidence

Instead of simply traveling at the flow rate of the fluid in the saturated zone, radionuclides will potentially undergo physical and chemical interactions that must be characterized to predict large-scale transport behavior. These interactions include molecular diffusion into the rock matrix, sorption on the minerals along the fractures or within the rock matrix, or transport in colloidal form. These phenomena will be described below.

When a dissolved species travels with the fluid within a fracture, it may potentially migrate by molecular diffusion into the stagnant fluid in the rock matrix. When a molecule enters the matrix, its velocity effectively goes to zero until the Brownian motion carries it back into the fracture or into an adjacent fracture. The result is a delay of the arrival of the solute at a downgradient location from what would be predicted if the solute had remained in the fracture. In hydrologic tests not involving tracers, the pore water velocity can often be estimated given assumptions about the fracture porosity. For interpreting hydrologic tests, the fracture porosity is usually the correct porosity value because pump testing is controlled by fracture flow. However, the groundwater travel time is often computed by dividing the flow path length by this velocity. This estimate is potentially a severe underestimate of the time required for a water molecule to migrate along the flow path. A more accurate definition of travel time for the purpose of predicting transport behavior would take into account matrix diffusion.

There have been several theoretical, laboratory, and field studies performed to demonstrate the validity of the matrix-diffusion model. Grisak and Pickens (1980) and Neretnicks (1980) first applied mathematical models to demonstrate the likely effect of matrix diffusion in flow in

fractured media. In these studies, transport was idealized as plug flow within the fracture with diffusion into the surrounding rock matrix. Sudicky et al. (1985) applied a similar model to a laboratory experimental apparatus in which tracer was injected into a thin sand layer with surrounding low permeability silt layers, showing that matrix diffusion was necessary to model the conservative tracer data. Neretnicks et al. (1982) reached the same conclusion in their experiments of transport in natural fissures in granite. Rasmuson and Neretnicks (1986) extended the concept of matrix diffusion to examine the coupling between matrix diffusion and channel flow usually thought to occur within natural fractures.

Transport models incorporating matrix-diffusion concepts have also been proposed to explain the often conflicting groundwater ages obtained from ^{14}C data compared to ages predicted from flow data. Sudicky and Frind (1981) developed a model of flow in an aquifer with diffusion into a surrounding aquitard to show that the movement of ^{14}C can be much slower than predicted if only movement with the flowing water is considered. Maloszewski and Zuber (1985, 1991) reach a similar conclusion with a model for ^{14}C transport that consists of uniform flow through a network of equally spaced fractures with diffusion into the surrounding rock matrix between the joints. Their model also includes the effect of chemical exchange reactions in the matrix, which further slows the migration velocity. Maloszewski and Zuber (1985) also present analyses of several interwell tracer experiments that show that their matrix-diffusion model can be used to provide simulations of these tests that are consistent with the values of matrix porosity obtained in the laboratory and aperture values estimated from hydraulic tests. The results are in all cases superior to previous analyses that did not include matrix diffusion effects. Finally, of greatest relevance to the saturated zone beneath Yucca Mountain is the C-Wells reactive tracer test (Reimus and Turin, 1997), which demonstrated that models that incorporate matrix diffusion provide more reasonable fits to the tracer-experiment data than those that assume a single continuum. They demonstrated that a suite of tracers with different transport characteristics (diffusion coefficient, sorption coefficient) produced breakthrough curves that can be explained using a diffusion model

that assumes diffusion of tracers into stagnant or near-stagnant water. Finally, Waddell (1997) recently reported a similar result for nonsorbing tracers with different diffusion coefficients in a fractured-tuff tracer experiment at the NTS.

Thus, the theory of matrix diffusion is generally thought to be based on sound physical principles, and demonstrations of its effect have been shown in both laboratory-sized specimens and interwell tracer tests. The effect on transport under groundwater flow conditions could be extremely large and, thus, should be incorporated into any realistic radionuclide migration model.

Data from naturally occurring isotopes such as ^{14}C provide valuable clues into the processes controlling transport in the saturated zone. In the present study, these data sets are best used in the development of conceptual models rather than as observations used directly in formal calibration exercises. The reasons for this approach are twofold. First, there is considerable uncertainty in the conceptual model of saturated-zone flow that gives rise to the data set. Waddell et al. (1984) observe that the hydrologic conditions that describe modern-day conditions, with recharge presumed to occur at higher elevations, is probably not correct for the climatic conditions during the Pleistocene Epoch. Yet many of the water ages in the saturated zone imply an origin of these fluids during the Pleistocene. The water ages near Yucca Mountain span a wider range, from 2–4 ky at UE-29 a#1 and #2 to 13 ky at USW H-1 with even higher values in other wells. Given that the chemical signature of the recharge fluid was probably much different during the Pleistocene and that more widespread recharge and discharge areas were present, the application of steady-state models to simulate the data is problematic.

Even if steady-state models could be used, the spatial scale of all groundwater flow models except the regional-scale model are insufficient to model ^{14}C without assumptions about the nature of flow outside the model domain. In principle, ^{14}C should be simulated as a chemical species that enters the groundwater at known recharge points with a modern signature and, through radioactive decay and possibly rock-water interactions, results in lower concentrations within the model. The site-scale model, designed to simulate flow and radionuclide transport at smaller scales, does not

cover the areal extent needed to set these boundary conditions, and the assigning of partially decayed ^{14}C concentrations for the fluid entering the model domain would be difficult.

Instead of using ^{14}C data as a calibration measurement, we take into account the ages at the level of conceptual model development. The ages of saturated-zone fluids are on the order of several thousand years or more. If transport through the saturated zone were isolated only to fractures, the effective porosity of the medium would be on the order of 0.001 to 0.0001, depending on fracture density and aperture. For the flow rates thought to be present in the saturated zone, solutes would transport from recharge areas to their present locations (sampling wells where ^{14}C is measured) in about 10 to 100 years. This result is clearly inconsistent with the measured ages in the saturated zone. If we assume that the age reflects the time it took for a solute to travel from a distant recharge point to the sampling location, then much higher effective porosities are required. This argument is consistent with the conceptual model of interchange of solutes between the fractures and matrix found in the matrix-diffusion model.

The fact that matrix diffusion appears to be consistent with the conceptual model does not imply that the fracture and matrix fluids must therefore be in chemical equilibrium at all locations in the saturated zone. The model is consistent with different chemical compositions in the fracture and matrix fluid. This situation would occur if the fracture spacing is sufficiently large that a solute traveling through fractures has insufficient time to diffuse fully within the matrix block between fractures. In reality, a spectrum of different transport regimes is probably present in the saturated zone, from fracture-dominated transport at some locations to complete equilibration between fracture and matrix fluids at other locations. The ^{14}C data constrain this possibly wide range of behavior by establishing that significant communication between fractures and matrix is likely.

5.5.3 Dispersion

Dispersion is caused by heterogeneities at all scales from the pore scale to the scale of the thickness of individual strata and the length of structural features such as faults. The resulting spreading and dilution of radionuclides is important to performance and must be captured in

transport models. The largest heterogeneities are represented explicitly in the site-scale model in that these features are embodied in the hydrogeologic structure on which the model is built. For dispersion at smaller scales, we assume that the convective-dispersion model applies with dispersion characterized using an ellipsoid aligned with the flow direction. Below, we address the validity of such an approach and potential shortcomings. For now, we focus on the parameters that must be assigned in the model to capture smaller-scale dispersion: the longitudinal and transverse dispersivities.

Transport field studies have been conducted at a variety of length scales from meters to kilometers to address the issue of dispersion. Figure 5-1, adapted from Neuman (1990), shows estimated dispersivity as a function of length scale. The clear trend is toward larger apparent dispersion coefficients for transport over longer distances. Solute samples larger-scale heterogeneities at larger scales, and thus spreading is more pronounced. Also shown in Figure 5-1 is a black diamond representing the dispersivity determined by Reimus and Turin (1997) for the C-Wells reactive tracer experiment. There is uncertainty in this estimate due to uncertainty in the exact flow path(s) taken by a tracer during the test. Nevertheless, the estimate falls within the range of the compiled data from other sites, suggesting that transport in the fractured tuffs exhibits similar dispersive characteristics. The values used in the simulations of radionuclide transport are somewhat higher than those estimated from the C-Wells because of the larger scale that is relevant for radionuclide migration to the accessible environment. Very little experimental information exists for assigning transverse dispersivity. In the present study, the "rule-of-thumb" value of one-tenth the longitudinal dispersivity is used.

When interpreting the results of numerical simulations using a dispersion model such as this, the reader must be aware of the inherent uncertainties and potential limitations. There are numerous studies using stochastic modeling approaches to capture smaller-scale heterogeneities within otherwise coarse descriptions of a flow and transport field. The virtue of these approaches is that the uncertainty of transport processes such as dispersion are automatically quantified in that the coefficients of the equations solved contain parameters related to the uncertainty. More formal

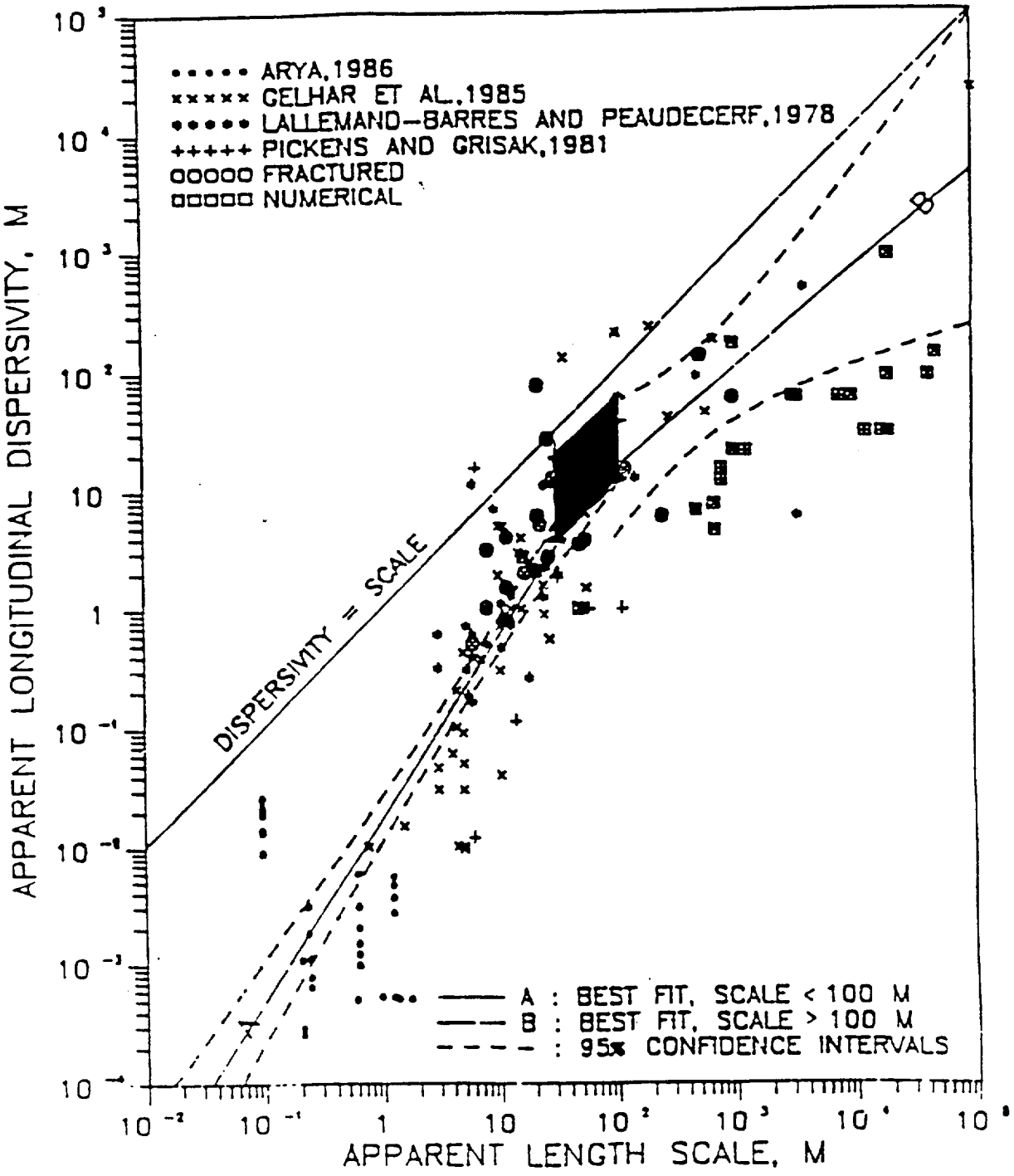

Adapted from Neuman (1990)

Figure 5-1. Dispersivity versus scale for various field sites and the C-Wells reactive tracer tests.

approaches to uncertainty such as these should be examined and possibly used in future iterations of the site-scale transport modeling studies. For now, we perform a series of deterministic simulations and vary the dispersivity as a sensitivity analysis.

This caveat on the validity of dispersive transport models must be remembered when interpreting the results. When attempting to capture all dispersion mechanisms at scales smaller than the size of a typical grid cell with a simple dispersion model, certain features likely to be present in reality are only simulated in an average sense. For example, suppose the actual system has a localized, high-permeability pathway within the domain defined by a grid cell. This region may have high concentration within the pathway and lower concentrations in the rest of the domain. A continuum model averages these differences, and a single value of concentration is defined for the block. A key issue then is whether a concentration value computed in the model actually represents a value likely to be found in any particular parcel of water in the saturated zone. Actually, concentration in averaged models such as this really represent the expected value of concentration in the vicinity of a given location. In other words, the computed concentration is proportional to the *probability* of radionuclide being present. Concentration differences at scales smaller than the grid cell are not resolved and may, in fact, be present.

Whether this distinction is important depends on specific performance criteria and scenarios for exposure to humans or plants. Well-withdrawal scenarios should take into account that the concentration a well accesses may have higher (or lower) concentration than is reported at a given location in the site-scale model. Although this appears to add an additional level of complexity and uncertainty to the performance analysis, it must be considered when using the results for performance predictions.

5.5.4 Other Transport Processes

Sorption of radionuclides on rock surfaces is another mechanism that will result in retardation. These radionuclide-rock interactions can potentially occur on the surfaces of fractures and within the rock matrix. This distinction is important because the surface-area to fluid-volume

ratio and the mineral distributions are probably different in the fractures as compared to the matrix. The lithium tracer in the C-Wells reactive tracer experiment was modeled by Reimus and Turin (1997) using a matrix-diffusion model with the sorption coefficient as an additional adjustable parameter. The matrix sorption coefficient that fit the data agreed quite well with the value determined in laboratory sorption tests, thus providing an additional degree of confidence in the matrix-diffusion model. The fact that the early lithium response had the same timing as that of the nonsorbing tracers, but with a lower normalized peak concentration, is consistent with matrix diffusion coupled with sorption in the matrix.

Transport of radionuclides on colloidal particles or in colloidal form is a third mechanism that may apply at the field scale. Colloidal particles have the potential to provide a direct pathway through fractures. Strongly sorbing radionuclides such as plutonium may adhere to these particles and transport more rapidly than if the radionuclide were confined to the aqueous phase. The size of the colloids will minimize diffusion into the rock matrix, thereby negating one possible retardation effect. On the other hand, filtration of colloidal material is likely to come into play, thereby resulting in large retardation factors. The key uncertainties in predicting colloid transport in the field are:

- determining whether a continuous pathway exists with large enough pore size to facilitate transport over large distances without filtration or migration into stagnant fluid storage, and
- the uncertainty regarding the relative amount of radionuclide on colloid surfaces versus that in the aqueous phase.

For the first uncertainty, field demonstration of colloidal transport is necessary to prove that this mechanism is important at the field scale. Furthermore, given the complexities of the interactions of colloids with the surrounding rock and geochemical conditions, further laboratory work to characterize these effects is necessary. A first step in this study has also been taken in the C-Wells experiment in which polystyrene microspheres were injected and breakthrough curves at the producing well were determined. The breakthrough times of the microspheres were similar to

those of the aqueous tracers, but the peak concentrations (on a normalized basis) were lower for the spheres. This result suggests some sort of retention mechanism, such as filtration, sorption, or settling of the particles. Given that these tests were conducted over a flowing distance of roughly 30 m, reduction in concentration over such distances may suggest that filtration or other retardation mechanisms will minimize the ability of colloids to travel the kilometer distances to the accessible environment. However, more work needs to be done using microspheres or other colloidal tracers to confirm this result.

5.6 Matrix Diffusion Mathematical Model

This section develops a mathematical model coupling fluid flow and solute transport in the fractured tuffs of the saturated zone. The model is of sufficient complexity to examine the importance of various parameters in predicting radionuclide transport. Thus, the goals of this modeling are to provide guidance on the most important processes affecting migration. We can then incorporate the results into the site-scale model in which additional complexity is introduced by the three-dimensional flow and transport pathways.

For present purposes, we propose a two-dimensional model shown schematically in Figure 5-2. Advection and dispersion occur within a set of parallel, equally spaced fractures, with interaction by molecular diffusion with the rock matrix. For axial dimension L much larger than the fracture spacing S, one-dimensional diffusion in the direction perpendicular to fluid flow is adequate. Reversible sorption is assumed to occur with possibly different values of the sorption-isotherm parameters for the fracture surface and the matrix. Due to symmetry, only transport in half of a single fracture and one-half of one matrix block needs to be considered (the shaded area in the figure). The set of equations resulting from a mass balance on a water-borne radionuclide are given below.

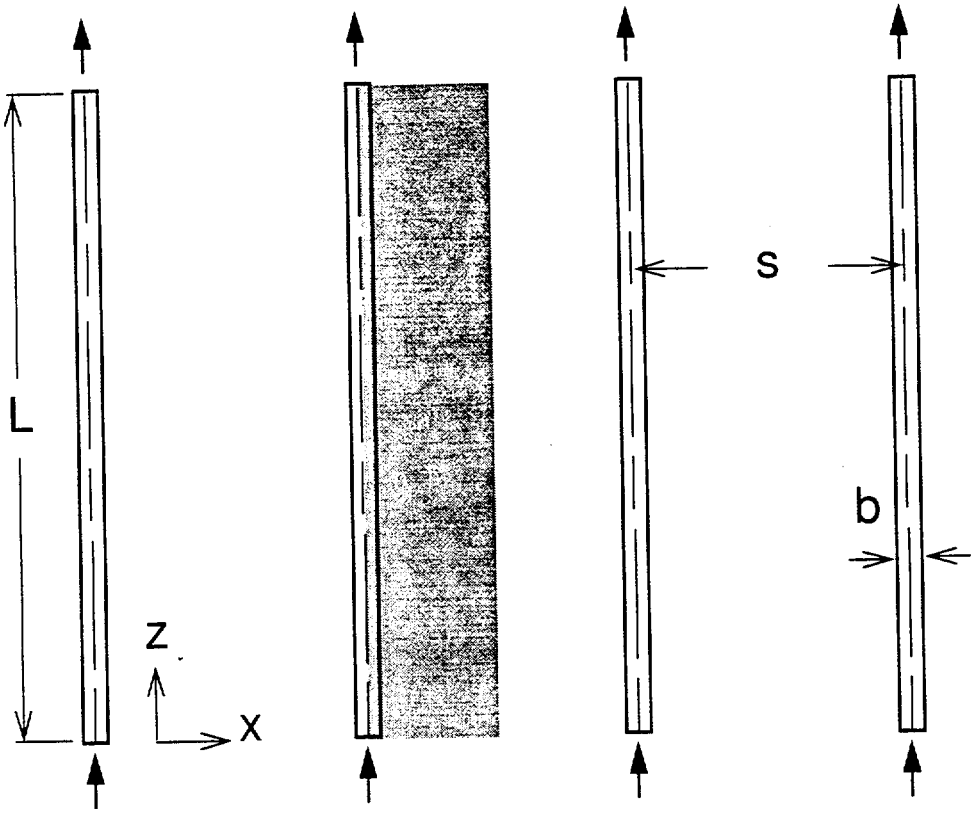

Figure 5-2. Schematic of matrix-diffusion model.

In the fractures:

$$\frac{\partial C}{\partial t} + \frac{v}{R}\frac{\partial C}{\partial z} - \frac{D}{R}\frac{\partial^2 C}{\partial z^2} + \frac{q}{bR} = 0 \quad , \qquad \text{(Eq. 5-1)}$$

where C is the concentration, t is time, v is velocity of the fluid, z is the direction along the fracture, D is the dispersion coefficient in the fracture, b is the half-aperture, R is the retardation factor in the fracture, and q is the diffusive flux from fracture to matrix described below.

In the matrix:

$$\frac{\partial C}{\partial t} - \frac{D_m}{R_m}\frac{\partial^2 C}{\partial x^2} = 0 \quad , \qquad \text{(Eq. 5-2)}$$

where D_m is the molecular diffusion coefficient, R_m is the retardation factor in the matrix, and x is the direction perpendicular to the fracture.

The concentration in the fracture is coupled to the concentration in the matrix via the diffusive flux term q given by

$$q = -\phi D_m \left.\frac{\partial C}{\partial x}\right|_{x=b} , \qquad \text{(Eq. 5-3)}$$

where ϕ is the porosity.

The boundary and initial conditions in the fracture are:

$$C(0,t) = C_o, \qquad \text{(Eq. 5-4)}$$

$$C(\infty,t) = 0, \qquad \text{(Eq. 5-5)}$$

$$C(z,0) = 0, \qquad \text{(Eq. 5-6)}$$

and for the matrix, the boundary and initial conditions are:

$$C(b,z,t) \text{ in the matrix} = C(z,t) \text{ in the fracture}, \qquad \text{(Eq. 5-7)}$$

$$\left.\frac{\partial C}{\partial x}\right|_{x=S/2} = 0 , \qquad \text{(Eq. 5-8)}$$

where S is the spacing between fractures and

$$C(x,z,0) = 0 . \qquad \text{(Eq. 5-9)}$$

In the present study, the finite-element heat and mass transfer code FEHM will be used to simulate flow and transport in this simplified system. A finite-element mesh was developed to simulate transport in the shaded region in Figure 5-2. The grid consists of 53 grid points in the flow direction and 30 grid points perpendicular to the fracture. The grid points along the flow path are equally spaced except for finely spaced regions near the inlet and outlet. The grid points in the matrix are very finely spaced close to the fracture (on the order of 1 mm), increasing as we proceed to the center line between fractures. This grid allows the details of the diffusional process to be accurately simulated both at short times, when the diffusional front in the matrix has not traveled very far from the fracture, and at long times, when the solute has had ample time to diffuse fully to the center line. Flow is confined to the fracture by setting extremely small permeabilities in the rock matrix.

The solution of this system of equations for a given location in the fracture is given as Equation 35 in Tang et al. (1981) for the case of a single fracture in an infinite medium, for which Equation 5-8 above is replaced by $C(\infty, z, t) = 0$. This solution is valid for the problem specified above until such time as the solute diffuses to the center line between fractures. At the other extreme, when the tracer diffuses fully to the center line over the time scale of transport along the fracture, a simple one-dimensional axial dispersion model is applicable with the porosity equal to the sum of the fracture and matrix porosities rather than just the fracture porosity (Maloszewski and Zuber, 1991). The grid spacings and time steps selected for the simulations were verified by obtaining excellent agreement between the finite-element code and analytical solutions for both the early-time (Tang et al.,1981) and late-time (one-dimensional axial dispersion equation) extremes.

Some of the inherent assumptions in the above equations must be justified in light of the discussion on hydrology presented above. First, the qualitative picture for dispersion presented in the hydrologic conceptual model was one of large-scale heterogeneities causing the dispersion. However, the mathematical model prescribes a constant and identical dispersion coefficient within each fracture. We are assuming that for a parametric study, it is adequate to assign a large value of dispersivity within each fracture corresponding to the values typically measured in the field rather than solving a multidimensional model with randomly distributed fractures or permeabilities. This assumption is justified because the primary focus of these simulations is to examine the coupling between fractures and matrix and its effect on radionuclide transit time. Multidimensional models are being developed that address the phenomenon of dispersion in a more realistic fashion. In any event, uncertainty in the dispersivity affects the spreading of the radionuclide front but not the mean arrival time. Thus, differences in the arrival times for models with and without matrix diffusion can be ascribed to matrix diffusion effects.

Using the parallel-plate model to represent the fracture is another assumption seemingly at odds with the conceptual model. Again recognizing for a parametric study the need to examine the relative importance of advection in fractures versus diffusion into the rock matrix, the idealized

model should be adequate as long as an appropriate value of aperture b is chosen. In this case, the aperture enters into the equations from the point of view of solute mass balance. Therefore, an average value of the "storage aperture," rather than the hydraulic aperture measured in hydraulic tests, is appropriate. Furthermore, the extent of matrix diffusion depends on the size of the aperture and the distance between fractures compared to the diffusional length scale, and thus, the true mean aperture is needed rather than one determined from a hydraulic measurement. The reason for stressing this distinction is that the storage aperture (fluid volume in a fracture divided by the fracture surface area) can be many times larger than the hydraulic aperture, which is heavily influenced by flow constrictions and channeling (e.g., Gelhar, 1987; Long and Billaux, 1987; Robinson, 1988). The implications of flow channeling within fractures must also be discussed. Flow within a portion of each fracture is equivalent, in a parametric sense, to a larger fracture spacing than implied by the geometry in Figure 5-2. The fracture-spacing parameter s therefore includes intricacies of flow through tortuous, channeling pathways.

To understand the model results to be presented, a dimensional analysis is appropriate. The phenomenon of matrix diffusion can be conceptualized as one in which various physical length scales can be compared to the characteristic diffusional length scale δ_d given by

$$\delta_d = \sqrt{D_M \times GWTT} \quad , \qquad \text{(Eq. 5-10)}$$

where D_M is the matrix diffusion coefficient and $GWTT$ is the groundwater travel time. Figure 5-3 is a schematic of the various transport regimes based on the dimensional analysis. In zone 1, δ_d is small or of the same magnitude as the fracture aperture, and thus, the transport time is given roughly by the groundwater travel time ($GWTT$). In zone 3, δ_d is as large or larger than the fracture spacing, and the solute is allowed to "sample" all of the pore space in the fracture and matrix. For this extreme, the transport time t_s is (Maloszewski and Zuber, 1991):

$$t_s = \frac{\phi_f + \phi_m}{\phi_f} \times GWTT \quad . \qquad \text{(Eq. 5-11)}$$

In most cases, $\phi_m \gg \phi_f$ and $GWTT$ can be multiplied by the ratio of the porosities to obtain the trans-

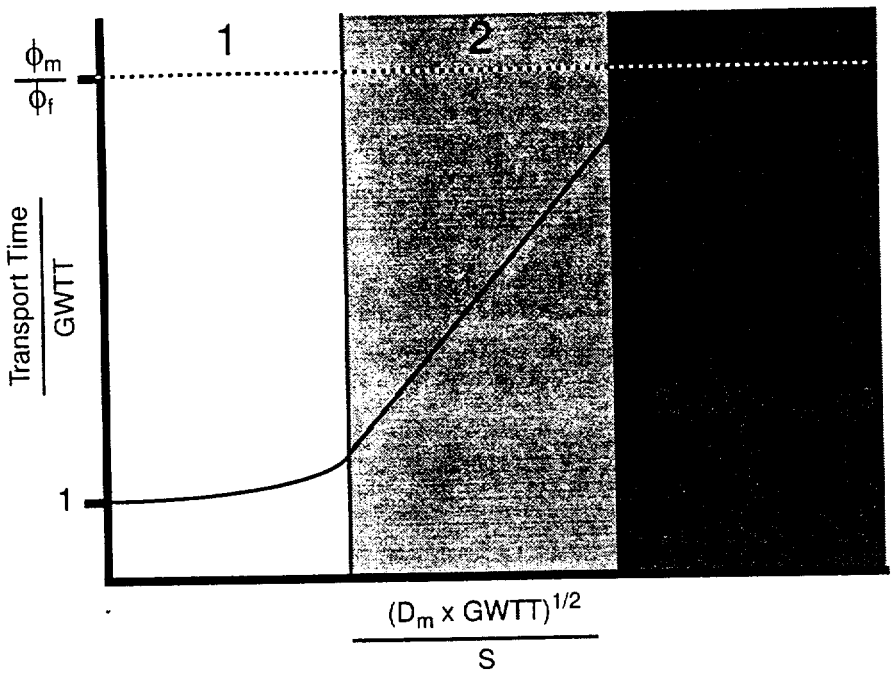

Figure 5-3. Schematic of the different regimes present in the matrix-diffusion model. The ordinate parameter relates the transport time of a solute to that in the absence of matrix diffusion. The abscissa variable is a dimensionless travel time.

port time. Zone 2 is an intermediate region in which the solute diffuses between the fractures but has insufficient time to reach the center line between fractures, where it mixes with solute from an adjacent fracture. The transition from Zone 1 to Zone 2 is controlled by the fracture aperture $2b$.

The goal of the numerical simulations is to establish which regimes are relevant for natural groundwater flow and forced gradient experiments in the saturated zone at Yucca Mountain. Figure 5-4 summarizes the results of numerous simulations in which *GWTT*, fracture spacing, and diffusion coefficient are varied at a constant matrix porosity of 0.05, and the fracture aperture $2b$ = 1 mm. In each simulation, a step change in inlet tracer concentration was imparted at t = 0, and the transport time is defined as the time required for the concentrations at the outlet of the fracture to reach one-half of the inlet value. The three transport regimes clearly show up in these

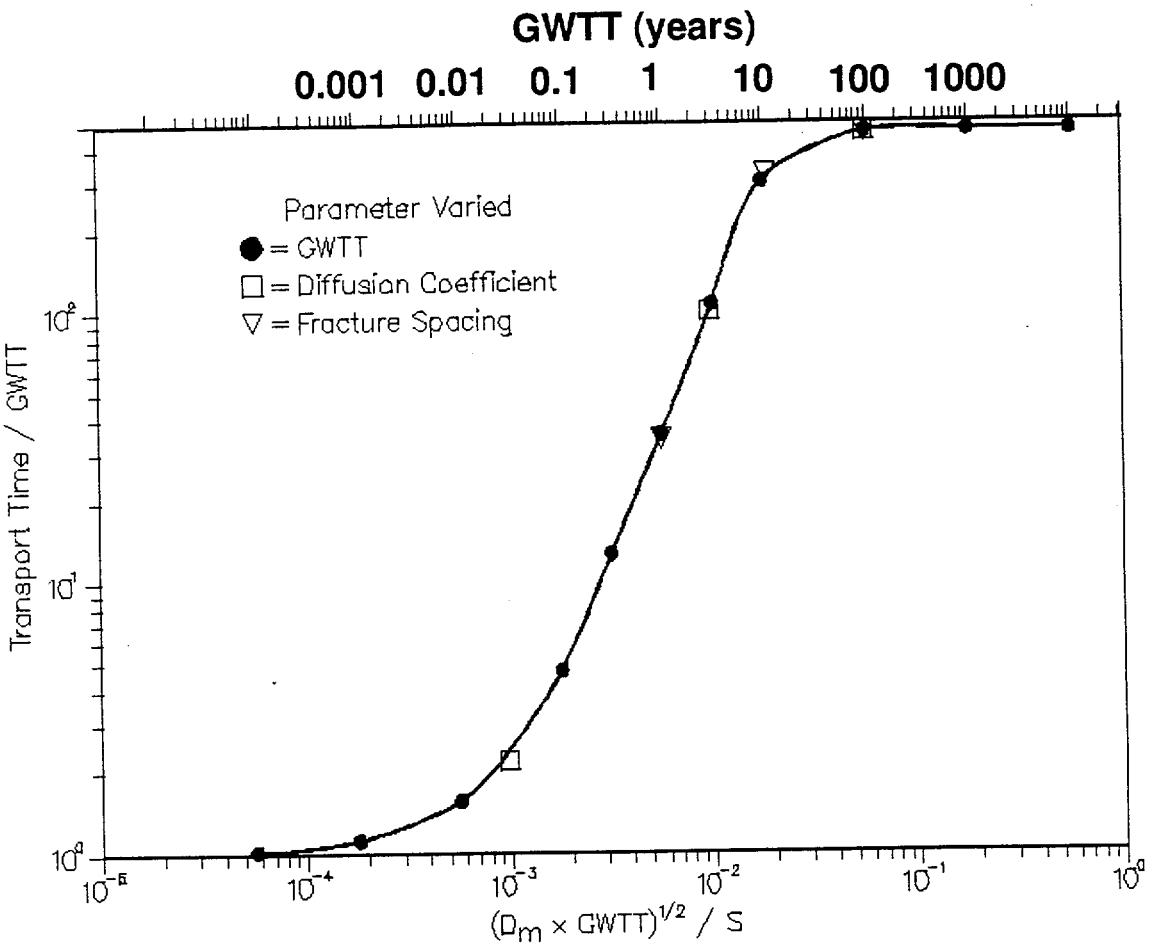

Figure 5-4. Results of matrix-diffusion model simulations, illustrating the enhanced travel times (above *GWTT*) predicted as a function of diffusion coefficient, fracture spacing, and *GWTT*.

simulations, which span the range of behaviors described schematically in Figure 5-3. For the simulations in which *GWTT* is varied at a fracture spacing of 10 m and $D_m = 10^{-10}$ m^2/s (a typical value for solutes in the Yucca Mountain tuffs, from Triay et al., 1997), the *x*-axis above the plot shows *GWTT* for each simulation. For all reasonable values of *GWTT* in the saturated zone at Yucca Mountain, the simulations are clearly in transport regime 3 in which the solute can diffuse fully between fractures. Only at *GWTT* of 10 years or less does the transport time depart significantly from a value of $\frac{\phi_m}{\phi_f} \times GWTT$. Thus, under these conditions the matrix-diffusion model suggests that radionuclide transport times could be several orders of magnitude higher than

GWTT itself. Although this conclusion is a result of the particular parameter values chosen, it is valid, but to a lesser degree, for conditions less favorable for matrix diffusion. In fact, lowering of the term $(\sqrt{D_m \times GWTT})/S$ by several orders of magnitude is required before matrix diffusion effects become negligible and *GWTT* can be used as the estimate of solute transport time.

Although the terminology developed above presumes that the model is being used to evaluate groundwater transport, the same calculations can be used to assess the impact of matrix diffusion on interwell field tests. In this case, *GWTT* is the distance between wells divided by the flow velocity within the fractures. If we take one day (2.74×10^{-3} years) as a rough estimate of this time, then the transport time will be increased by about a factor of 2 from the interwell *GWTT*. This fact suggests that field tests with tracers should be influenced by matrix diffusion, though at a lower level than for contaminant transport under natural flow conditions. This result is in fact corroborated in the C-Wells experiments in which the extent of matrix diffusion, though discernible, is limited compared to that predicted under natural gradients because of the much shorter travel times in an interwell test.

The results of Figure 5-4 suggest an approximate method for assigning appropriate values for "transport porosity," the effective porosity suitable for capturing the travel time of a solute in a porous continuum model. The value in the ordinate can be thought of as the ratio of the effective porosity to the fracture porosity, and it can be used as a multiplier to the fracture porosity to obtain an effective porosity for transport. The basis for this simplification is that, if this porosity is assumed, the median travel time from the matrix-diffusion model will be reproduced. Thus, to a first approximation, the travel time through the medium will be properly predicted with this effective porosity. We use this concept in Chapter 6 to test the sensitivity of the model to details of the matrix diffusion process. Specifically, we use effective porosity values ranging from a presumed fracture porosity of 10^{-4} to the matrix porosity values.

5.7 Colloid Transport Mathematical Model

In this section, we include a simplified colloidal transport-model equation to derive a combined aqueous/colloidal transport model. The key assumptions of the colloidal transport sub-model are:

- the contaminant sorbs reversibly to the colloids in addition to interacting with the rock matrix and fractures;
- the colloids are isolated to the fracture and possess dispersive properties equivalent to that of an aqueous solute; and
- the colloids interact reversibly with the fracture surface.

Given these assumptions, a transport equation for contaminant attached to colloids can be written as

$$R_c \frac{\partial C_c}{\partial t} = D \frac{\partial^2 C_c}{\partial z^2} - v \frac{\partial C_c}{\partial z} \quad , \qquad \text{(Eq. 5-12)}$$

where C_c is the concentration of contaminant attached to colloids and R_c is a retardation factor that captures the details of colloid attachment/detachment and filtration processes.

To couple the transport equation for contaminant on colloids (Equation 5-12) to the aqueous transport equation (Equation 5-1), reversible, linear sorption of contaminant onto colloids is assumed:

$$C_c = K_c C \quad , \qquad \text{(Eq. 5-13)}$$

where K_c is the distribution parameter relating the concentrations. Because both C and C_c are expressed as moles contaminant per unit fluid volume, K_c is a dimensionless parameter expressing the ratio of contaminant mass residing on colloids to the mass present in aqueous form. In terms of more commonly defined and measured quantities, K_c is the product of the distribution coeffi-

cient for contaminant on colloids and the concentration of colloidal material available for sorption (mass of colloids per unit fluid volume). Adding Equations 5-1 and 5-12, and making use of Equation 5-13, we obtain for the concentration of the contaminant in the aqueous phase for the fracture:

$$\left(\frac{R + K_c R_c}{1 + K_c}\right)\frac{\partial C}{\partial t} = D\frac{\partial^2 C}{\partial z^2} - v\frac{\partial C}{\partial z} - \frac{q}{b(1 + K_c)} \quad . \qquad \text{(Eq. 5-14)}$$

The coupling between the fracture and matrix is identical to the case without colloids, because we assume no mobility of colloids into the matrix rock. Inspection of Equations 5-1 and 5-14 reveals that the forms of the transport equations are identical with different constants in the accumulation and diffusive loss terms. Therefore, the numerical solutions presented in the previous section still apply, and the parameters need only be interpreted differently to include colloid contaminant transport. To do this, we define revised constants $\hat{R}$ and $\hat{b}$ as follows:

$$\hat{R} = \frac{R + K_c R_c}{1 + K_c} \quad \text{and} \qquad \text{(Eq. 5-15)}$$

$$\hat{b} = b(1 + K_c) \quad . \qquad \text{(Eq. 5-16)}$$

Using these expressions instead of their counterparts R and b allow us to consider colloidal transport. Qualitatively, there are two impacts of colloid-facilitated transport. First, Equation 5-15 implies that the retardation effect of sorption onto the matrix is reduced for nonzero values of K_c. In addition, in a mathematical sense, the system with colloid-facilitated transport behaves identically to one in which the effective fracture aperture is larger by a factor of $1 + K_c$. This result effectively expands Zone 1 in Figure 5-3. In the limit of large values of K_c, the system behaves as one with little or no matrix diffusion, and the effective transport porosity equals the fracture porosity. This limiting behavior is used in Chapter 6 to simulate colloid-facilitated transport of plutonium.

5.8 Conclusions

A conceptual model was described that includes advective transport of radionuclides, dispersion, diffusion of radionuclides from fractures into the rock matrix, sorption, and colloid-facilitated transport. Within the fractured tuffs, the migration of radionuclides is expected to be primarily through regions with higher bulk fracture permeability. Flow within individual joints probably occurs through channels rather than as sheet flow through parallel-plate fractures. At more distant downstream locations, the migration is likely to be through alluvium, and a model for flow and transport through a porous continuum, rather than a fractured rock, is likely to apply. It was shown that transport can be approximated using an effective transport porosity that, in general, falls between the fracture porosity and the porosity of the surrounding rock matrix. The matrix-diffusion model is shown to be consistent with ^{14}C ages measured for saturated-zone fluids, although the data do not rule out some differences in concentration between fracture and matrix fluids. Dispersion is caused by heterogeneities at all scales from the pore scale to the scale of the thickness of individual strata and the length of structural features such as faults. The resulting spreading of radionuclides is important to performance and must be captured in transport models. Only the largest heterogeneities are represented explicitly in the site-scale model; all dispersion caused by smaller-scale features must be represented through the use of a dispersion model.